IS-T-464

MAGNETOELASTIC EFFECTS IN TERBIUM AND DYSPROSIUM

Ph. D. Thesis Submitted to Iowa State University, August 1971

Dennis Thomas Vigren

Ames Laboratory, USAEC
Iowa State University
Ames, Iowa 50010

Date Transmitted: September 1971

PREPARED FOR THE U. S. ATOMIC ENERGY COMMISSION
DIVISION OF RESEARCH UNDER CONTRACT NO. W-7405-eng-82

DISCLAIMER

IS-T-464

Available from: National Technical Information Service
Department A
Springfield, VA 22151

Price: Microfiche $0.95

Magnetoelastic effects in terbium and dysprosium

by

Dennis Thomas Vigren

A Dissertation Submitted to the

Graduate Faculty in Partial Fulfillment of

The Requirements for the Degree of

DOCTOR OF PHILOSOPHY

Major Subject: Solid State Physics

Approved:

S. H. Liu
In Charge of Major Work

For the Major Department

For the Graduate College

Iowa State University
Ames, Iowa
August 1971

TABLE OF CONTENTS

Magnetoelastic effects in terbium and dysprosium

Dennis Thomas Vigren

ABSTRACT

A detailed theoretical study has been made of the magnetoelastic perturbation of the spectra of elementary spin and lattice excitations in Tb and Dy metals. The theory was formulated on the basis of an interaction formed from bilinear products of local spin and strain functions. Previous ad hoc models appear in certain limits of the theory, giving a coherence to the theoretical picture of magnetoelastic coupling. It is found that uniform magnetostriction causes a smooth transition from "free lattice" to "frozen lattice" perturbation of the magnon spectrum depending on the wavevector of the state.

The microwave absorption versus magnetic field applied along the hard planar axis of Tb and Dy is calculated. It is found that free lattice magnons are primarily responsible for low frequency absorption in Tb below 140 K, and for both low and high frequency absorption in Dy below the Curie temperature of that metal. It is shown that the transition from free to frozen lattice behavior of the magnon spectrum is essential to the explanation of existing data on the temperature dependence of absorption peak positions in Tb.

The dynamic interaction between spin and lattice waves is derived, and used to calculate the mixed-mode splittings in regions of the Brillioun zone of Tb where phonon and magnon dispersion curves cross. The theory predicts well the splitting which occurs where the acoustical magnon and phonon branches touch, but fails to account for the splitting between the acoustical magnon and optical phonon branches.

INTRODUCTION

The rare earth metals, particularly Tb and Dy, are found to strain considerably in the ferromagnetic state. This distortion is roughly two orders of magnitude larger than that induced in transition metal ferromagnets. Straining causes changes in the crystalline field and in the crystal potential as seen by the conduction electrons. These in turn cause changes in the magnetic anisotropy and exchange coupling experienced by the spin system. For a particular ordered configuration of the spins, the crystal tends to distort so as to minimize the free energy. Magnetically induced strain is called magnetostriction, and the coupling between spins and strains is called the magnetoelastic interaction.

The magnetoelastic interaction plays an important role in determining the order of the magnetic ground state of Dy metal. It is also responsible for other ground state phenomena, such as anomalous thermal expansion, and changes in the elastic constants when magnetic ordering occurs. The interaction also has a profound effect on the elementary excitations of the spin and lattice systems.

Two adhoc models have been proposed for the way in which ferromagnetic spin waves of Tb and Dy metals are influenced by magnetostriction. One presupposes that for long wavelength excitations of the spin system the macroscopic strain can follow at each instant of time the motion of the nearly uniform spin oscillations; it is termed the "free lattice" model. The other presupposes that such strains cannot follow the spin oscillations at all and that the spins vibrate against the strain field produced by the ground state ferromagnet; it is termed the "frozen lattice" model.

The calculated field dependence of the long wavelength energy gap in the magnon spectrum of ferromagnetic Tb and Dy is strikingly different for the two models. For the free lattice model, the gap can be reduced to zero by an application of a magnetic field of suitable size along the hard planar axis; for the frozen lattice model, the gap is reduced to a minimum value which is roughly proportional to the square root of the magneto-elastic interaction. The two models have been tested experimentally using neutron diffraction and microwave absorption techniques. The neutron diffraction work and high frequency FMR substantiate the frozen lattice model; whereas, the low frequency microwave work can only be explained on the basis of a free lattice model.

It is the main purpose of this work to calculate the magnetoelastic contribution to the magnon spectrum, beginning from first principles, with a realistic microscopic picture of the magnetoelastic coupling. It is shown that the magnon states vary smoothly from free to frozen lattice behavior depending upon the wavelength of the excitation. By looking carefully into the way in which the neutrons and microwaves excite the magnetic system, a consistent explanation of all experimental results is attained.

As a further application of the microscopic model of the magneto-elastic coupling, a calculation of magnon-phonon mixing is made. The results are compared with spectrum splittings observed in Tb metal. The mixing of acoustical or optical excitations is well explained by the theory; but the theory does not account for the mixing of unlike modes

(e.g., acoustical magnons with optical phonons). An alternate mechanism which may cause this mixing is given in the Appendix.

SURVEY OF PAST RESEARCH ON RARE EARTH MAGNETISM

Early studies of the magnetic properties of solids were made on the transition metals of the iron group as they exhibit strong ferromagnetism at room temperature. The microscopic model of such metals, however, is quite complicated because the wave functions of the 3d electrons which are responsible for magnetism are neither completely localized on atomic sites nor are they well described by Bloch waves. Rare earth metals, on the other hand, can be treated as Heisenberg ferromagnets to a first approximation. This fact has motivated extensive experimental investigation of these metals, despite their typically low ordering temperatures.

A good model for rare earth metals consists of a lattice of tri-positive ions immersed in a sea of 6s and 5d conduction electrons. The tri-positive ions have an unfilled 4f shell which gives rise to a net magnetic moment localized on the ions. The magnetic moments approximate closely the free ion value predicted by Hund's rule. This is due to the fact that 4f wavefunctions on neighboring ion sites do not overlap because the 4f electrons are buried deep in the atomic core and are shielded from neighboring ions by filled 5s and 5p shells. Since there is negligible 4f overlap between ions, direct exchange coupling of the local moments is insignificant. Rather, ordered states are produced by an indirect exchange process. The 4f electrons couple to the conduction electrons by Coulombic exchange. Treating this exchange interaction as a pertubation, a Heisenberg exchange interaction between local moments is obtained in second order.

An improvement on this basic model of rare earth magnetism takes account of the magnetic anisotropy experienced by the local moments. Such anisotropy arises from the interaction of the moments with the crystalline electric field, or with local strain fields. The latter type of coupling is called the magnetoelastic interaction, and the bulk of this treatise will be concerned with its description and consequences.

The heavy rare earths (i.e., those whose 4f shell is half or more than half full) possess the hexagonal close-pack structure. Although the hcp structure is not simple, it is far simpler than symmetries exhibited by the light rare earths. Also, a comparison of magnetic behavior among the heavy rare earths is facilitated by the fact that they have the same lattice point group symmetry. These facts have made them the primary object of investigation. An intensive study of the ground state magnetic structure of the heavy rare earths was made in 1961 by the Oak Ridge National Laboratory by neutron diffraction methods in which spiral, cone, as well as other exotic spin structures were discovered (1).

Tb and Dy were found to have a particularly simple planar spiral periodicity along the hexagonal axis. The ionic moments, confined to the basal plane by strong axial crystal field anisotropy, are aligned ferromagnetically within a given hexagonal plane. The direction of planar alignment rotates as a function of position along the hexagonal axis producing a spiral structure. In addition to the simplicity of the periodic order, these metals exhibit a transition to simple ferromagnetism which make them very useful in the study of the mechanisms which stabilize a particular spin structure.

Periodic magnetic structures arise because the indirect exchange coupling J_{ij} between spins $\vec{S}_i$ and $\vec{S}_j$ is a long-range, oscillatory function of the spin separation (2). The stable spin configuration is that which minimizes the free energy. In temperature regions where the exchange energy is the dominant term in the free energy, it may be shown (3) that the energy of a magnetic structure with periodicity $\vec{q}$ is proportional to $-\chi(\vec{q})$, the generalized susceptibility. The quantity $\chi(\vec{q})$ represents the linear response of the conduction electrons to the effective magnetic field of the ionic moments, and can be expressed in terms of the conduction electron energy bands, $\epsilon_{k,n}$, in a Bravais lattice as follows (4):

$$\chi(\vec{q}) = \frac{1}{N} \sum_{\vec{k},n,n'} \left[\frac{f_{\vec{k}n}\,(1 - f_{\vec{k}+\vec{q}+\vec{Q}'\,n'})}{\epsilon_{\vec{k}+\vec{q}+\vec{Q}'\,n'} - \epsilon_{\vec{k}n}} \right] ,$$

where n and n' are band indices, $\vec{k}$ is the reduced wavevector of the electrons, $\vec{Q}'$ is a reciprocal lattice vector necessary to put $\vec{k} + \vec{q}$ into the first Brillioun zone, $f_{\vec{k}n}$ are the Fermi-Dirac distribution functions, and N is the number of atoms in the lattice. Realistic band calculations have been performed on the heavy rare earths, and wavevectors which maximize the generalized susceptability are shown to correspond to the wavevectors of the observed ground state magnetic order in Gd, Dy, Er, and Lu (5).

Enz (6) originally proposed an explanation of the spiral to ferromagnetic order transition observed in Dy at 87 K on the basis of an energy balance between the total exchange energy which favors a spiral spin

structure and other mechanisms which favor ferromagnetism. Such mechanisms are the rather small planar anistropy in Dy and Tb (7) which favors alignment of moments along a preferred or "easy" axis in the basal plane, and the magnetoelastic interaction which also favors ferromagnetism. The transition should then occur at a temperature where the competing energies are equal. The temperature dependence of the planar anisotropy and of the magnetoelastic energy was first predicted theoretically (8,9) and subsequently measured (7,10,11). Analysis of these results shows clearly that it is the magnetoelastic energy which competes effectively with the exchange interaction in Dy in the region of the Curie temperature, and which precipitates the transition to ferromagnetism (5).

Thus, from a decade of experimental and theoretical effort, a rather clear picture of the ground state magnetism of the heavy rare earths has emerged. The next logical step was to study the excited states (spin waves) of these ordered systems. A spin wave excitation is just a natural mode of vibration of the spin system about its equilibrium configuration. The term "magnon" denotes a quantum of the spin wave field.

Cooper, Elliott, Nettel, and Suhl (12) derived the spectrum, $E(\vec{q})$, of ferromagnetic magnons using a model in which the spins were coupled by exchange, and interacted individually with the crystal field and an externally applied magnetic field, $\vec{H}$. For Tb and Dy metals with $\vec{H}$ applied in the "hard" planar direction, they predicted that the exchange interaction was responsible for the dispersion of E, and that a magnetic anisotropy of crystal field origin gave rise to a gap at zero wavevector which could be reduced to zero upon application of a magnetic field of

appropriate strength.

The theory of Cooper et al. neglects any effects of the magnetoelastic interaction which was found to be so important in the understanding of ground state magnetic ordering. If one assumes a "free lattice" model for the spin-strain coupling, neglect of the lowest order magnetoelastic terms (i.e., those terms quadratic in the components of magnetic moment) is justifiable. Such terms are invariant to a rotation of the magnetization in the basal plane. In Tb and Dy the spin oscillations are confined to this plane by strong axial anisotropy. Therefore, in the event that the macroscopic strain field can adjust freely to the spin motion (i.e., free lattice model), no magnetoelastic energy arising from lowest order coupling is spent to excite the spin system. Cooper (13) later calculated the effects of second order magnetoelastic terms in the free lattice model (i.e., terms of fourth power in the components of magnetization and possessing hexagonal symmetry). He again found that magnetic anisotropy gave rise to a zero field gap which could be reduced to zero by the application of an appropriate magnetic field. In this case, however, the magnetic anisotropy in the basal plane arose from a combination of crystal field and second order magnetoelastic effects.

In 1966 Turov and Shavrov (14) predicted that a large contribution to the magnon gap was possible from the lowest order magnetoelastic coupling terms under the assumption of a "frozen lattice." A frozen lattice is one which cannot respond at all to the spin oscillations in an excited state. In this case, the spins vibrate against the macroscopic strain field produced by the ground state ferromagnetism, creating

magnetoelastic energy, and giving rise to a gap of magnetoelastic origin.

Cooper (13) calculated the magnon spectrum under the assumption of such a frozen lattice, and applied the results to Tb and Dy. He found that the magnetoelastic interaction made a sizable contribution to the gap. He calculated the behavior of the gap in an applied field, and found that the gap could not be reduced to zero by application of a field in the hard planar direction. Instead, the gap dips to a minimum value which is roughly proportional to the square root of the magnetoelastic energy. Thus, Cooper's calculations predicted a radical difference in the applied field behavior of the magnon gap between the frozen and the free lattice models.

Much experimental interest was created by the theoretical speculations and calculations, and numerous microwave ferromagnetic resonance studies were performed on Tb and Dy to ascertain whether the frozen or free lattice model was correct. One method was to measure the temperature dependence of the gap in zero field, since the temperature dependence of the crystal anisotropy and magnetoelastic terms are well known. This was done by Marsh and Sievers (15) who found that both the free and frozen lattice models fit their data well, although the frozen lattice model fits slightly better.

A measurement of the applied field behavior of the gap is a much more conclusive test of the proposed models. Such measurements on Tb and Dy metals were performed by Bagguley and Liesegang (16), Rossol (17,18), Wagner and Stanford (19,20) and Hart and Stanford (21) using ferromagnetic resonance techniques. A variable dc field is applied in the hard planar direction

and a fixed microwave frequency photon beam is incident normal to the surface of the metal. As the applied field is increased, the uniform mode spin wave dips and then increases. Strong coupling of the photons to the spin waves occurs when the frequencies are equal. Microwave energies far below the zero field spin wave gap are used so that if E(0) dips to zero, and the free lattice model is valid, then strong on-resonance absorption of the photons should occur at some field; whereas, if the gap cannot be reduced to the very low microwave energies, and the frozen lattice model is valid, one should see only broad off-resonance absorption over a considerable range of the applied field. This off-resonance absorption is possible only because the magnon spectrum is broadened allowing spin waves in the tail of the energy distribution to couple to the microwaves.

Bagguley and Liesegang measure strong absorption of 1.8 K and 0.45 K microwaves in Tb and Dy. The absorption is characterized by a sharp increase which might be expected in the case of on-resonance absorption, followed by a long tail spanning many kilo-Oersteds of field. The tail is characteristic of broad off-resonance absorption. Rossol did a very detailed investigation of Dy with 1.8 K microwaves. Wagner studied both Tb and Dy using 0.45 K and 4.5 K radiation. The observations of these workers agreed essentially with those of Bagguley and Liesegang. The observation of strong and sudden absorption of 0.45 K and 1.8 K photons cannot be understood using a frozen lattice model which implies only off-resonance absorption at these low driving frequencies. The profile of such absorption would be very broad and flat with no sudden change in slope,

quite unlike the observed profiles (16,17,20,21). Thus, low frequency FMR results seem to argue against the applicability of a frozen lattice. Other microwave experiments (19) at higher frequencies (4.5 K) show a temperature dependence of the resonance field in agreement with the frozen lattice model. At these higher frequencies, on-resonance absorption is possible even if the lattice is frozen.

Recently, Mackintosh (22) in a neutron diffraction study of the magnon gap of Tb in an applied field obtains excellent agreement with the predictions of the frozen lattice model. He not only reports that the energy gap could not be reduced to zero upon application of a strong field in the hard planar direction of ferromagnetic Tb, but also that the field dependence of the gap agrees with the frozen lattice theory over a large temperature range.

Thus, one is confronted with experimental observations which appear to be contradictory. Neutron diffraction results clearly conclude that the lattice is frozen. High frequency resonance absorption also indicates a frozen lattice; but low frequency resonance absorption cannot be explained unless the lattice is free. It is unreasonable to believe that a crystal can respond totally to a frequency of 40 GHz (1.8 K), but not at all to a frequency twice as great.

In this work the spin-wave spectrum is studied, assuming that spins are coupled locally to their strain environments. Thus, no a priori assumption is made as to whether the macroscopic strains are free or frozen. The resulting spectrum is shown to vary continously from free to frozen lattice behavior depending on the wavevector of the magnon. A

A consistent understanding of all existing spin-wave data can be attained by considering in detail the spin disturbance created in a particular experiment, and to what extent the various magnon states are populated.

THE MAGNETOELASTIC INTERACTION

Spin-lattice coupling arises because the magnetic interactions are sensitive to the ionic positions, and so are modulated by distortions of the crystal. For a given ordered spin state the energy difference between the strained and unstrained lattice is called the magnetoelastic energy. A net strain (magnetostriction) will always result if the magnetic system is ordered. Since the spin-lattice coupling mechanisms are varied and complex, a phenomenological approach is used in which the general form of the interaction is written down with coupling coefficients to be determined experimentally.

Callen and Callen (9) imposed symmetry and simplicity conditions on the form of such an interaction. They required it to be linear in the strain components since the magnetostriction is quite small compared to crystal dimensions. Since terms linear in the spin components would not be time reversal invariant, they coupled the strain components to spin functions quadratic in the spin components. Since the Hamiltonian must be invariant under operations of the crystal point group, linear combinations of the Cartesian components of spin and strain are taken in order to form basis functions of the irreducible representations of the crystal point group. Callen and Callen treat the strains as classical quantities and assume them to be uniform. The spin functions involve spin components on either one or two sites and are termed 1-ion or 2-ion spin functions, respectively. The 1-ion interactions describe strain modulation of the interaction of individual spins with their local environments (e.g., the

crystalline electric field or applied magnetic field); the 2-ion interactions describe strain modulation of the interaction between spin pairs (e.g., Heisenberg exchange or dipole-dipole coupling). The phenomenological magnetoelastic Hamiltonian may then be written as a sum of 1-ion and 2-ion terms (9):

$$H_{me} = -\sum_{f}\sum_{\Gamma}\sum_{jj'} \tilde{B}^{\Gamma}_{jj'}(f) \sum_{i} \epsilon_i^{\Gamma j} S_i^{\Gamma j'}(f)$$

$$-\sum_{(f,g)}\sum_{\Gamma}\sum_{jj'} \tilde{D}^{\Gamma}_{jj'}(f,g) \sum_{i} \epsilon_i^{\Gamma j} S_i^{\Gamma j'}(f,g) \quad . \qquad (1)$$

Here f,g are position indices, Γ labels the irreducible representations of the crystal point group, i specifies the basis set of the representation, j and j' are used if more than one basis set carries the representation, ϵ's are linear combinations of uniform strain components, S(f) and S(f,g) are the 1-ion and 2-ion spin functions, and B(f) and D(f,g) are the 1-ion and 2-ion magnetoelastic coupling coefficients. Note that other terms of higher degree in the spin components may be included, but they are of higher order than those written in Equation (1) (23,24). The total elastic Hamiltonian is then:

$$H_e = H_{me} + \frac{1}{2}\sum_{\Gamma}\sum_{jj'} c^{\Gamma}_{jj'} \sum_{i} \epsilon_i^{\Gamma j} \epsilon_i^{\Gamma j'} \quad , \qquad (2)$$

where the c's are the elastic constants.

The coupling coefficients $\tilde{B}$ and $\tilde{D}$ are determined experimentally.

Suppose $\frac{\delta \ell_o}{\ell_o}$ is the fractional change in length of the crystal measured in a direction specified by direction cosines $(\beta_x \beta_y \beta_z)$. Then if $\bar{\epsilon}_{\mu\nu}$ are the equilibrium Cartesian components of strain in the presence of magnetic order, it can be shown (25) that:

$$\frac{\delta \ell_o}{\ell_o} = \sum_{\mu,\nu} \bar{\epsilon}_{\mu\nu} \beta_\mu \beta_\nu \quad . \tag{3}$$

The equilibrium strains $\bar{\epsilon}_{\mu\nu}$ are determined by minimizing the quantum statistical average of the total elastic Hamiltonian H_e with respect to the strain components. For the case of hexagonal symmetry, substitution of the equilibrium strains into Equation (3) yields (9):

$$\frac{\delta \ell_o}{\ell_o} = \frac{1}{3} \lambda_{11}^{\alpha} + \frac{1}{2\sqrt{3}} \lambda_{12}^{\alpha} \left(\alpha_z^2 - \frac{1}{3}\right) + 2\lambda_{21}^{\alpha} \left(\beta_z^2 - \frac{1}{3}\right) + \sqrt{3} \lambda_{22}^{\alpha} \left(\alpha_z^2 - \frac{1}{3}\right)$$

$$\left(\beta_z^2 - \frac{1}{3}\right) + 2\lambda^{\gamma} \left[\frac{1}{4} \left(\alpha_x^2 - \alpha_y^2\right)\left(\beta_x^2 - \beta_y^2\right) + \alpha_x \alpha_y \beta_x \beta_y \right] +$$

$$2\lambda^{\epsilon} \left(\alpha_y \alpha_z \beta_y \beta_z - \alpha_x \alpha_z \beta_x \beta_z\right) . \tag{4}$$

The $\lambda_{jj'}^{\Gamma}$'s are called magnetostriction constants and contain the temperature independent magnetoelastic coupling coefficients $\tilde{B}$ and $\tilde{D}$ (linearly), the elastic constants, and the temperature dependent quantum statistical spin averages. The vector $(\alpha_x, \alpha_y, \alpha_z)$ defines the direction of the magnetization and should not be confused with the α-representations of the hexagonal point group. The irreducible representations of the hexagonal

group, their dimensions, and their basis functions are summarized in Table 1.

Table 1. Irreducible representations of the hexagonal group, their dimensions, and their basis functions

Irrep	Dimension	Basis Functions
$\alpha 1$	1	$x^2 + y^2 + z^2$
$\alpha 2$	1	$\frac{\sqrt{3}}{2}(z^2 - \frac{1}{3}r^2)$
γ	2	$\frac{1}{2}(x^2 - y^2)$, xy
ϵ	2	xz, yz

The magnetostriction constants are measured experimentally by repeated use of Equation (4) with different sets $(\vec{\alpha}, \vec{\beta})$. Typically $\vec{\alpha}$ is varied by application of an external field and $(\vec{\beta})$ by the use of strain gauges affixed to the sample at different orientations relative to the crystal axes. The coupling coefficients can be extracted from the zero temperature limit of the magnetostriction constants, and the temperature dependence of the magnetoelastic energy is contained in them.

Callen and Callen (26) have derived an essentially model independent temperature and field renormalization for spin averages of the l-ion type. If one lets ℓ denote the degree of the spin operator to be averaged, then the ratio of the average at temperature T and field H to that at zero temperature and field is equal to $\hat{I}_{\ell+\frac{1}{2}}(x)$ where $\hat{I}_{\ell+\frac{1}{2}}(x)$ is the ratio of the

hyperbolic Bessel function of order $\ell + \frac{1}{2}$ to that of order $\frac{1}{2}$, and x is the inverse Langevin function of the reduced magnetization σ. That is, $\sigma\ (T,H) = \coth x - 1/x$. Experimentally, in Tb and Dy the behavior of the magnetostriction constants are predicted well by the 1-ion temperature theory with the exception of λ_{11}^{α} and λ_{21}^{α} which are quite small (27). The temperature dependence of 2-ion averages has been worked out using a two-spin cluster theory with nearest and next-nearest neighbor exchange (28). This theory applies well to europium chalcogenides (e.g. EuO and EuS) in which the exchange coupling is short ranged, but is not applicable to rare earth ferromagnets in which the exchange is long ranged. In applications with Tb and Dy below, it is assumed that the magnetoelastic energy is described well by the 1-ion temperature theory.

The formalism of Callen and Callen, successful as it was in treating the thermally averaged aspects of magnetoelastic coupling in ferromagnets, is not sufficiently general to describe such coupling in antiferromagnets where the magnetostriction is non-uniform. In the description of dynamic spin-lattice coupling their formalism is also totally inadequate because it treats the strains as classical and spacially uniform, and therefore precludes a calculation of the magnon-phonon mixing.

Evenson and Liu (5) generalized the formalism of Callen and Callen by coupling the local spin functions to local strain functions. The Cartesian components of these local strains are defined as follows:

$$\varepsilon_{xx}\ (f,g) = (X_f - X_g)(x_f - x_g),$$

$$\varepsilon_{xy}\ (f,g) = \frac{1}{2}\ [(X_f - X_g)(y_f - y_g) + (Y_f - Y_g)(x_f - x_g)], \qquad (5)$$

and similarly for the other 2-ion Cartesian components. Here $\vec{R}_f = (X_f, Y_f, Z_f)$ is the position vector of the $f^{\underline{th}}$ ion in the unstrained crystal; $\vec{r}_f = (x_f, y_f, z_f)$ is the displacement of the $f^{\underline{th}}$ ion from its unstrained position. In applications to Dy and Tb, the z-axis of the Cartesian coordinates is taken along the crystal c-axis, and the x-axis is taken along the easy planar direction. The 1-ion strains are defined simply by contraction on one of the position indices: $\mathcal{E}(f) = \sum_g \mathcal{E}(f,g)$. The strain functions are defined according to conditions of symmetry and simplicity. They are chosen to be linear in the components of displacement, symmetric under interchange of site labels, and to form a 3 x 3 symmetric matrix.

The local magnetoelastic interaction is then represented by the following Hamiltonian:

$$H_{me} = -\sum_f \sum_\Gamma \sum_{jj'} B^\Gamma_{jj'}(f) \sum_i \mathcal{E}_i^{\Gamma j}(f)\, S_i^{\Gamma j'}(f)$$

$$-\sum_{(f,g)} \sum_\Gamma \sum_{jj'} D^\Gamma_{jj'}(f,g) \sum_i \mathcal{E}_i^{\Gamma j}(f,g)\, S_i^{\Gamma j'}(f,g) \quad . \qquad (6)$$

This Hamiltonian allows for the coupling of spins to the local distortions of the crystal. It reduces to the Hamiltonian of Callen and Callen when the spins are ferromagnetically aligned; and such a reduction establishes the relation between the coupling coefficient of the two theories (5).

Evenson and Liu used the local magnetoelastic coupling theory to compute the way in which a lattice distorts in the presence of a helical spin structure. They found that the bulk of the lattice remains unstrained

and that local, periodic distortion of the lattice persists only within a surface layer of the crystal. This effect is termed "lattice clamping" and was first recognized by Cooper (29). The thickness of the surface layer in which local lattice distortion is possible is proportional to the spacial periodicity of the spin alignment. The clamping effect was experimentally verified in Dy which shows an orthorhombic distortion in the ferromagnetic phase (30), but no such distortion in the helical phase. It also reduces the negative elastic free energy in the helical phase of Dy, making the ferromagnetic state elastically more stable, and finally precipitating a transition at the Curie temperature (5).

FERROMAGNETIC SPIN WAVES IN Tb AND Dy METALS

The Long Wavelength Spectrum at Zero Temperature and Field

The displacements $\vec{r}_f$ which appear in the local strain functions consist of two parts. One gives rise to magnetostriction produced by the spin order; the other gives rise to normal modes of vibration about the strained equilibrium positions. In this section we treat the effect of the magnetostriction, which shifts the magnon energy spectrum. In a later section we treat the coupling of spin and lattice vibrational modes in the production of mixed mode states. In treating the effects of magnetostriction we initially assume that the lattice is infinite, and that the crystal is capable of responding so as to produce macroscopic strains that minimize the elastic energy. Later we refine the theory so as to account for finite crystal dimensions and a limited response time.

The clamping effect described in the last section is essential to understanding the way in which magnetostriction affects the spin wave energies. When a spin precesses about its equilibrium position, it tends to drag the lattice distortion with it. For a spin wave of infinite wavelength, the lattice distortions of all unit cells move in phase, so that they add up to a macroscopic strain which follows the precession of the magnetization. Clearly, the strain configuration relative to the magnetization direction is identical at each instant of time to that of the ground state ferromagnet. That is to say, it costs no magnetoelastic energy to excite the spin system, and the energy gap at zero wavevector is due solely to the magnetic anisotropy produced by the crystal field.

This situation corresponds to a free lattice model for the magnetoelastic coupling. In the event that a spin wave of finite wavelength is excited, the periodic spin component induces only a periodic distortion at the surface of the crystal. For a wavelength equal to the thickness of the crystal, the penetration of the distortion is complete. For some shorter wavelength, however, the distortion is sufficiently confined to the surface of the crystal so that the bulk strain is induced by the ferromagnetic spin component. This volume strain is essentially the same as that produced by the ground state magnetization, and is constant in time. The spins now oscillate about this fixed strain axis creating magnetoelastic free energy and giving rise to a magnetoelastic contribution to the energy gap. This situation corresponds to the frozen lattice model. Thus, the lattice behavior varies from free to frozen lattice within a very small range of $\vec{q}$, where $\vec{q}$ is the wavevector of the magnons. Under the assumption of an infinitely large specimen, this rapid variation results in a discontinuity in the magnon spectrum from $\vec{q} = 0$ to $\vec{q} = 0^+$, where $\vec{q} = 0^+$ is taken to mean the shortest finite magnon wavevector as determined by the inverse dimensions of the specimen.

This discontinuity is now calculated quantitatively for Tb and Dy which have the hexagonal close-packed structure (hcp). Since the magnetostriction arises from the ferromagnetically aligned components of the spins, we have the following reduction of the local strains (5):

$$\mathcal{E}^{\Gamma}(f) = 4a^2 \epsilon^{\Gamma} , \; B^{\Gamma}_{jj'}(f) = \tilde{B}^{\Gamma}_{jj'}/4a^2 \quad .$$

where ϵ^{Γ} is the usual uniform strain tensor, a is the hcp lattice parameter, and $\tilde{B}^{\Gamma}$ is the coupling coefficient in Callen and Callen notation. The 1-ion part of H_{me} is applied to the γ, ϵ, and $\alpha 2$ irreducible representations of the hcp point group, and the 2-ion part is applied to $\alpha 1$ (10). The sum on g is taken over nearest neighbors only, and the coefficients B^{Γ} and D^{Γ} are assumed to be independent of atomic site. From the quadratic form of the elastic energy density and the general form of Equation (6), the γ-terms in the strain dependent Hamiltonian are:

$$H^{\gamma} = \frac{c^{\gamma}}{2} [(\epsilon_1{}^{\gamma})^2 + (\epsilon_2{}^{\gamma})^2] + \tilde{B}^{\gamma} \sum_f (\epsilon_1{}^{\gamma} S_{f1}{}^{\gamma} + \epsilon_2{}^{\gamma} S_{f2}{}^{\gamma}) .$$

Minimizing this with respect to the strain components, we obtain :

$$H^{\gamma} = - \frac{(\tilde{B}^{\gamma})^2}{2c^{\gamma}} \sum_{ff'} (S_{f1}{}^{\gamma} S_{f'1}{}^{\gamma} + S_{f2}{}^{\gamma} S_{f'2}{}^{\gamma}) .$$

The spin functions are transformed to a coordinate system (ξ, η, ζ) in which ζ is along the equilibrium spin direction:

$$S^{\gamma}_{f1} = \frac{1}{2} [(S_f{}^{\zeta})^2 - (S_f{}^{\eta})^2],$$

$$S^{\gamma}_{f2} = \frac{1}{2} (S^{\zeta}_f S^{\eta}_f + S^{\eta}_f S^{\zeta}_f).$$

Applying the Holstein-Primakoff transformation in the small spin deviation approximation, we find:

$$S^{\gamma}_{f1} = \frac{S}{4} (2S-1 + a_f{}^{\dagger} a_f{}^{\dagger} + a_f a_f - 6 a_f{}^{\dagger} a_f),$$

$$S^{\gamma}_{f2} = \frac{\sqrt{2S}}{2i} S (a_f - a_f{}^{\dagger}) .$$

Now Fourier transforming the magnon operators and summing over lattice sites, we obtain:

$$\sum_f S^\gamma_{f1} = \frac{S(2S-1)N}{4} + \frac{S}{2} \sum_{\vec{q}} (\tau_{\vec{q}} - 6n_{\vec{q}}),$$

$$\sum_f S^\gamma_{f2} = -S\sqrt{NS}\, i\,(a_{\vec{0}} - a_{\vec{0}}^\dagger), \text{ where}$$

$$\tau_{\vec{q}} \equiv a_{\vec{q}}^\dagger\, a_{-\vec{q}}^\dagger + a_{\vec{q}}\, a_{-\vec{q}} ,$$

$n_{\vec{q}} \equiv a_{\vec{q}}^\dagger\, a_{\vec{q}}$, and $\vec{q}$ is the wavevector of the magnon.

In the last step we confine $\vec{q}$ to the first Brillouin zone. Here N is the number of atoms in the crystal. Then we have:

$$H^\gamma = \frac{(\tilde{B}^\gamma)^2 NS^2}{8c^\gamma}\,(2S-1) \sum_{\vec{q}} (6n_{\vec{q}} - \tau_{\vec{q}}) - \frac{(\tilde{B}^\gamma)^2 NS^3}{2c^\gamma}\,(2n_{\vec{0}} - \tau_{\vec{0}}), \quad (7)$$

where we keep only second order magnon terms. In an exactly similar manner we obtain:

$$H^\epsilon = -\frac{(\tilde{B}^\epsilon)^2 NS^3}{2c^\epsilon}\,(2n_{\vec{0}} + \tau_{\vec{0}}). \quad (8)$$

In treating the α-representation we let $(\delta_x, \delta_y, \delta_z)$ be the nearest neighbor position vector. Then the uniform part of the local strain is:

$$\mathcal{E}^{\alpha 1}_{f\delta} = \delta_x^2 \epsilon_{xx} + \delta_y^2 \epsilon_{yy} + \delta_z^2 \epsilon_{zz} + 2\delta_x\delta_y\epsilon_{xy} + 2\delta_x\delta_z\epsilon_{xz} + 2\delta_y\delta_z\epsilon_{yz},$$

$$\mathcal{E}^{\alpha 2}_{f\delta} = \frac{\sqrt{3}}{2}\,(\delta_y\delta_z\epsilon_{zy} + \delta_y\delta_z\epsilon_{zy} + \delta_z^2\epsilon_{zz} - \frac{1}{3}\,\mathcal{E}^{\alpha 1}_{f\delta}).$$

Here we used the uniform strain part of the local displacement. Now we transform from Cartesian components to basis functions of the α representation:

$$\mathcal{E}_{f\delta}^{\alpha 1} = \delta_0 \frac{\epsilon^{\alpha 1}}{3} - \delta_1 \frac{\epsilon^{\alpha 2}}{\sqrt{3}},$$

$$\mathcal{E}_{f\delta}^{\alpha 2} = \delta_2 \frac{\epsilon^{\alpha 2}}{6} - \delta_1 \frac{\epsilon^{\alpha 1}}{6\sqrt{3}} .$$

Here we use the notation:

$$\delta_0 \equiv \delta_x^2 + \delta_y^2 + \delta_z^2 ,$$

$$\delta_1 \equiv \delta_x^2 + \delta_y^2 - 2\delta_z^2 ,$$

$$\delta_2 \equiv \delta_x^2 + \delta_y^2 + 4\delta_z^2 .$$

The $\alpha 2$ term is of the "one-ion" type so summation over the nearest neighbors using the hcp geometry gives the expected reduction:

$$\mathcal{E}_f^{\alpha 2} = 4a^2 \epsilon^{\alpha 2}.$$

Computing the spin functions we obtain:

$$\sum_f S_{f\delta}^{\alpha 1} = NS^2 - 4S \sum_{\vec{q}} n_{\vec{q}} (1 - \cos \vec{q} \cdot \vec{\delta}),$$

$$\sum_f S_f^{\alpha 2} = - \frac{NS^2}{2\sqrt{3}} + \frac{\sqrt{3}S}{2} \sum_{\vec{q}} (2n_{\vec{q}} + \tau_{\vec{q}}).$$

Substitution of the spin and strain functions into the elastic Hamiltonian, summation over nearest neighbors in the two-ion Hamiltonian, and

minimization with respect to the strain components yield to second order in the boson operators:

$$H^{\alpha} = A_q^{\alpha} n_q + \frac{1}{2} B_q^{\alpha} \tau_q, \tag{9}$$

where

$$A_q^{\alpha} = -\sqrt{3}\, NS^3 \left[\frac{\tilde{B}_{12}}{c_{11}} \left(\tilde{B}_{11} - \frac{\tilde{B}_{12}}{2\sqrt{3}}\right) + \frac{\tilde{B}_{22}}{c_{22}} \left(\tilde{B}_{21} - \frac{\tilde{B}_{22}}{2\sqrt{3}}\right)\right]$$

$$+ NS^3 \left[\frac{1}{c_{11}} \left(\tilde{B}_{11} - \frac{\tilde{B}_{12}}{2\sqrt{3}}\right) \left(2\tilde{B}_{11} + \frac{\tilde{B}_{21}}{\sqrt{3}}\right) + \frac{1}{c_{22}} \left(\tilde{B}_{21} - \frac{\tilde{B}_{22}}{2\sqrt{3}}\right)\left(3\tilde{B}_{21} + 2\sqrt{3}\, \tilde{B}_{11}\right)\right]$$

$$\times \left(1 - \cos \frac{qc}{2}\right),$$

$$B_q^{\alpha} = -\sqrt{3}\, NS^3 \left[\frac{\tilde{B}_{12}}{c_{11}} \left(\tilde{B}_{11} - \frac{\tilde{B}_{12}}{2\sqrt{3}}\right) + \frac{\tilde{B}_{22}}{c_{22}} \left(\tilde{B}_{21} - \frac{\tilde{B}_{22}}{2\sqrt{3}}\right)\right],$$

where c is the hcp lattice parameter, and the subscripted c's refer to the elastic constants of the α representation. Here we have assumed $\vec{q} = q\hat{c}$, and will consider only magnon propagation in this direction throughout the remainder of this manuscript. The cosine dependent term is a direct consequence of the two-ion nature of the $\alpha 1$ representation. It arises from the fully symmetric magnetoelastic term, and so contributes a term in the total Hamiltonian identical in form to the Heisenberg exchange term. We have calculated the numerical value of the term using the data of Rhyne and Legvold (31), and find that it accounts for less than 10% of the magnitude of $(J_q - J_0)$ deduced from the spin wave data in the region of small q. Here J_q refers to the Fourier transform of the exchange energy.

Insufficient magnetostriction data were available on Dy metal to do a similar analysis, but one would expect a result similar to that of Tb. Thus, it seems safe to neglect the two-ion magnetoelastic interaction in the extraction of J_q from the spin wave spectrum of these metals.

Using the Equations (7), (8), and (9) and the results of Cooper (13) in treating the magnetic anisotropy terms in the spin Hamiltonian, we may write a partial Hamiltonian for magnons propagating along the c-axis as

$$H_m = \sum_q [A_q n_q + \frac{1}{2} B_q \tau_q], \tag{10}$$

where the sum is over wavevectors along the hexagonal axis in reciprocal space, and

$$A_q = 2S(J_0 - J_q) - P_2 S - 21 P_6^6 S^5 + A_q^{me},$$

$$B_q = -P_2 S + 15 P_6^6 S^5 + B_q^{me}.$$

Here P_6^6 and P_2 are the six-fold and two-fold anisotropy constants, respectively. The magnetoelastic terms are:

$$A_q^{me} = \frac{3c^\gamma (\lambda^\gamma)^2}{4NS} - [\frac{c^\gamma (\lambda^\gamma)^2}{2NS} + \frac{c^\epsilon (\lambda^\epsilon)^2}{2NS}] \delta_{q0} + A_q^\alpha,$$

$$B_q^{me} = -\frac{c^\gamma (\lambda^\gamma)^2}{4NS} - [\frac{c^\epsilon (\lambda^\epsilon)^2}{2NS} - \frac{c^\gamma (\lambda^\gamma)^2}{2NS}] \delta_{q0} + B_q^\alpha,$$

where λ^Γ are the conventional temperature dependent magnetostriction constants defined by Callen and Callen (9). The Kroneker delta is written to indicate that these terms appear only when q is identically zero.

The Hamiltonian H_m may be diagonalized by a transformation to new

boson operators and the energy spectrum of magnons with wavevectors $\vec{q} = q\hat{c}$ is given by:

$$E(q) = [(A_q + B_q)(A_q - B_q)]^{1/2}.$$

Let

$$\Delta_+ \equiv A_q^{me} + B_q^{me}$$

$$\Delta_- \equiv A_q^{me} - B_q^{me}.$$

In the limit of long wavelengths we must distinguish two cases:

1. At $q = 0$,

$$\Delta_+ = \frac{c^\gamma(\lambda^\gamma)^2}{2NS} - \frac{c^\epsilon(\lambda^\epsilon)^2}{NS} - \frac{\sqrt{3}}{NS}\{c_{11}[\lambda_{11}\lambda_{12} - \frac{(\lambda_{12})^2}{2\sqrt{3}}]$$

$$+ c_{22}[\lambda_{21}\lambda_{22} - \frac{(\lambda_{22})^2}{2\sqrt{3}}]\},$$

$$\Delta_- = 0.$$

2. At $q = 0^+$,

$$\Delta_+ = \frac{c^\gamma(\lambda^\gamma)^2}{2NS} - \frac{\sqrt{3}}{NS}\{c_{11}[\lambda_{11}\lambda_{12} - \frac{(\lambda_{12})^2}{2\sqrt{3}}]$$

$$+ c_{22}[\lambda_{21}\lambda_{22} - \frac{(\lambda_{22})^2}{2\sqrt{3}}]\},$$

$$\Delta_- = c^\gamma(\lambda^\gamma)^2/NS.$$

The γ terms in case 2 are identically the results of Cooper's frozen lattice calculation (13). (Cooper's expression for $\tilde{B}^\gamma$ in terms of λ^γ

should be multiplied by factor 2/3.) In case 1, Δ_- is identically zero so that the magnetoelastic coupling has little effect on the spin wave spectrum except through Δ_+ which appears in the factor with axial anisotropy. So case 1 agrees with the free lattice model which predicts negligible magnetoelastic perturbation of the magnon energies.

Table 2. Energy gaps for Tb at T = 0 K and Dy at T = 78 K

Metal	E(0)	$E(0^+)$
Tb	14.0 K	19.4 K
Dy	6.8 K	10.2 K

The numerical values of E(0) and $E(0^+)$ are given in Table 2 for Tb and Dy. In calculating these values, the data of Fisher and Dever (32) were used for the elastic constants, and the data of DeSavage and Clark (10) and Rhyne and Legvold (31) were used for the magnetostriction constants of Tb. The magnetostriction constants of Dy were taken from the data of Clark et al. (11). The free lattice gap is smaller than the frozen lattice gap as expected, and the discontinuity is quite significant in both metals. It should be remembered that this discontinuity is artificial due to the assumption of an infinite lattice; and that for a lattice of finite dimension there is a smooth transition from free to frozen lattice behavior as the magnon wavevector increases from zero.

In analyzing the data of neutron diffraction and ferromagnetic resonance, it is important to see which way the lattice behaves in the presence

of the magnetic disturbance created by the neutron or photon probes. An important consideration is over what macroscopic distance the uniform magnetostriction, which minimizes the instantaneous elastic energy, can be realized by the crystal. Since strain is a differential quantity, the deformation at any interior point $\vec{r}$ depends on the deformation of the surface atoms and its distance from the surface. Such information is carried from the surface with a velocity of 10^6 cm/sec in Tb (the speed of sound). Microwave and neutron diffraction experiments typically excite magnons of frequency 10^{10} cycles/sec so that only atoms within a distance of 10^{+4} Å of the surface can receive this information and can distort in accordance with the equilibrium strains. Thus, if the probe which creates the spin disturbance penetrates deeply into the crystal, as in the case of neutron diffraction, the bulk of the lattice cannot respond and remains frozen. Thus, one excites frozen lattice magnons in a neutron diffraction experiment. In ferromagnetic resonance on metals, however, the photons can only penetrate the surface a distance d called the radiation skin depth. In Tb and Dy this is about 10^4 Å for 10 GHz radiation so that macroscopic strains are easily formed in the region where the microwaves couple to the spin system, making free lattice behavior possible. It will be shown in a later section that the free lattice magnons are essential in the interpretation of microwave absorption experiments in which a large dc magnetic field is applied along the hard axis in the basal plane of a hexagonal close-packed metal.

The Long Wavelength Magnon Spectrum at Finite Temperature and Field

The temperature renormalization of the spin-wave spectrum is easily accomplished using the "one-ion" theory of Callen and Callen (9,26) described above. The magnetoelastic terms are renormalized according to $(\hat{I}_{5/2})^2$, where the function $\hat{I}_{5/2}$ is a reduced hyperbolic Bessel function, whose argument is the inverse Langevin function of the relative magnetization. This renormalization is not quite correct since the $\alpha 1$ representation should be renormalized according to a "two-ion" scheme. However, the $\alpha 1$ representation contributes only a small term to the factor in Equation (10) containing the large axial anisotropy term, $-2P_2S$, so that the result is negligibly affected by this error. The temperature renormalization of the planar anisotropy depends on the origin of this anisotropy. Recent neutron diffraction work by Mackintosh (22) showed that virtually all the planar anisotropy of Tb metal arises from hexagonally symmetric second order magnetostriction. Thus the renormalization should be $\hat{I}_{9/2}\ \hat{I}_{5/2}$ (13,9,26). In Dy metal, however, one might expect that the crystal field is more important in producing the anisotropy since Dy ions have a higher orbital angular momentum than Tb ions, and hence are capable of stronger interaction with the crystal field. We assume that the planar anisotropy of Dy arises solely from the crystal field interaction, and use the renormalization $\hat{I}_{13/2}$ (9,26). Then using an oblate spheroid geometry for the samples, we can generalize Equation (10) to the case of finite field and temperature (13):

$$E(q \sim 0) = \{[-2P_2 S\, \hat{I}_{5/2}\, \sigma^{-1} - 6P_6{}^6S^5 \cos 6\theta\, \hat{I}_{13/2}\, \sigma^{-1}$$

$$+ g\mu_B (H + 4\pi M - D_x M) \cos(\tfrac{\pi}{6} - \theta)$$

$$+ \Delta_+ \hat{I}_{5/2}{}^2\, \sigma^{-1}]\, [-36P_6{}^6S^5 \cos 6\theta\, \hat{I}_{13/2}\, \sigma^{-1}$$

$$+ g\mu_B H \cos(\tfrac{\pi}{6} - \theta) + \Delta_- \hat{I}_{5/2}{}^2\, \sigma^{-1}]\}^{1/2} \quad . \qquad (11)$$

The equation is written for Dy metal. In the case of Tb we make the replacement $\hat{I}_{13/2} \rightarrow \hat{I}_{9/2}\, \hat{I}_{5/2}$ in Equation (11) and all related formulae. D_x is a demagnetization factor, $\vec{M}$ is the net magnetization, σ is the relative magnetization, and θ is the angle between $\vec{M}$ and the easy axis in the basal plane. The angle θ is implicitly a function of the applied field, and is given as a solution to the transcendental equation (17):

$$\frac{\sin 6\theta}{6 \sin(\frac{\pi}{6} - \theta)} = \frac{g\mu_B H}{36P_6{}^6S^5 \hat{I}_{13/2}\, \sigma^{-1}} \quad .$$

The H that appears here and in Equation (11) is the external field. The relevant hyperbolic Bessel functions were evaluated in closed form using the recursion formulae found in the NBS Table of Functions. The final expressions used were:

$$\hat{I}_{5/2}(z) = 1 - \frac{3\sigma}{z} \quad ,$$

$$\hat{I}_{9/2}(z) = 1 + \frac{45}{z^2} + \frac{105}{z^4} - (\coth z)(\frac{10}{z} + \frac{105}{z^3}) \quad ,$$

$$\hat{I}_{13/2}(z) = (1 + \frac{210}{z^2} + \frac{4725}{z^4} + \frac{10395}{z^6}) - (\coth z)(\frac{21}{z} + \frac{1260}{z^3} + \frac{10395}{z^5}) .$$

Here $\mathcal{L}(z) = \sigma$ where $\mathcal{L}$ is the Langevin function.

The values of $\sigma(\vec{H},T)$ were taken from the isothermal magnetization curves of Behrendt and Legvold (33) for Dy, and of Hegland et al. (34) for Tb. These curves were plotted against the internal field so care was taken to convert to the external field, using the demagnetizing factors of an oblate spheroid.

The spin wave energies are plotted against the external field in Figures 1 and 2 for Dy and Tb, respectively. The curves are drawn for fields above the domain alignment field only. A strong dip in the free lattice mode, E(0), occurs when the external field approaches the effective planar anisotropy field. This effective field arises from magnetoelastic and crystal field anisotropy in the basal plane, and is represented by the applied field independent terms in the second factor under the radical sign in Equation (11). As the temperature increases, this effective field decreases until it falls below the domain alignment field of the sample. This occurs at 110 K for Dy, and at 140 K for Tb. The frozen lattice mode, $E(0^+)$, is rather flat over most of the field sweep in the low temperature ferromagnetic regimes of these metals. Also, this mode lies far above the applied microwave energies, which are indicated by horizontal lines in the Figures, with the exception of a sharp drop near the domain alignment field in Tb. Thus, at low temperatures one expects frozen lattice excitations to cause a broad off-resonance absorption spanning most of the field range with no sharp increase at the effective planar anisotropy field. On the other hand one expects strong on-resonance coupling of the free lattice modes to the microwaves near the

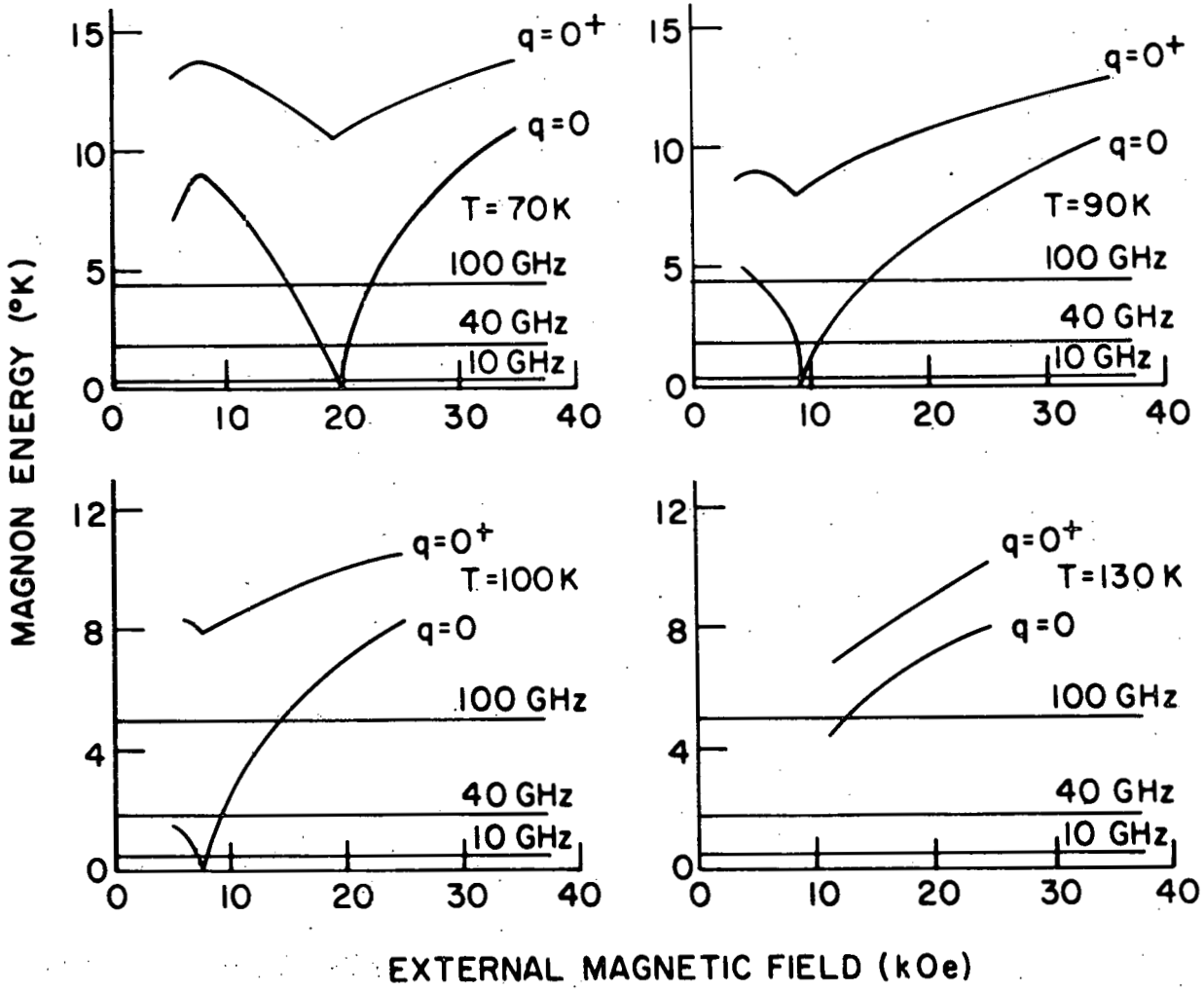

Figure 1. Magnon energy versus external magnetic field for dysprosium metal

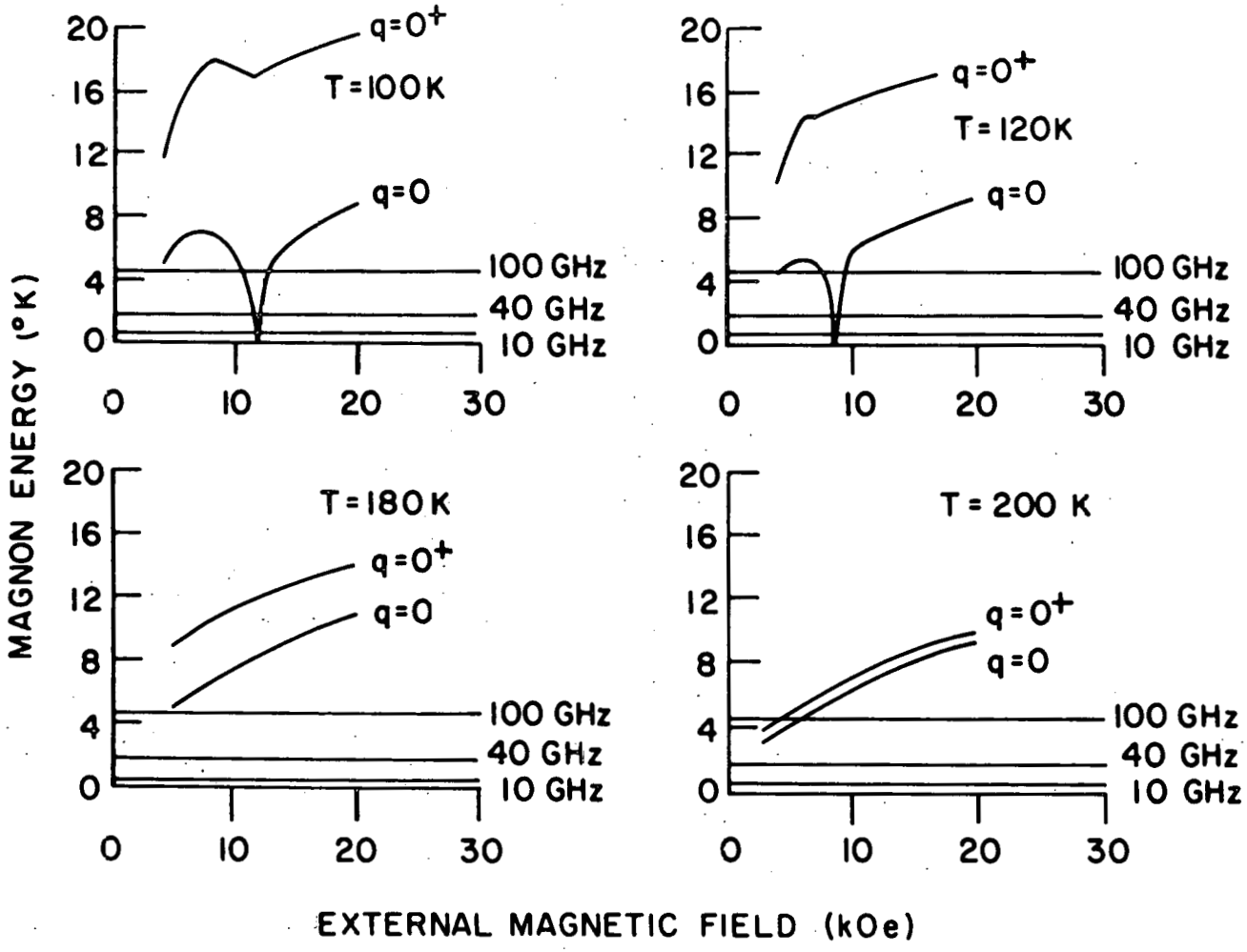

Figure 2. Magnon energy versus external magnetic field for terbium metal

planar anisotropy field. Rossol (17) observes strong absorption of 37 GHz radiation at 78 K, 86 K, and 91 K near the planar anisotropy field in Dy metal. In a recent microwave study at 24 GHz, Hart and Stanford (21) observe sharp absorption peaks near the planar anisotropy field between 70 K and 140 K in Tb metal. These experiments suggest strongly that the free lattice magnons are responsible for low frequency ferromagnetic resonance absorption. In the next section, a detailed calculation of microwave absorption is made for Dy and Tb, and the relative importance of the free and frozen lattice magnons to this process at various frequencies, temperatures, and applied fields is determined.

CALCULATION OF FERROMAGNETIC RESONANCE ABSORPTION PEAKS

In this section we calculate in detail the microwave absorption expected in resonance experiments in which a large dc magnetic field is applied along the hard axis in the basal plane of a hexagonal close-pack metal. Typically, these are the experiments of Bagguley, Rossol, Wagner, and Hart (16-21).

The experimental configuration is as shown in Figure 3. The crystal is cut so that the $\hat{c}$ direction is perpendicular to the metal surface. The photon beam is incident along this direction. The radiation is linearly polarized in the plane of the metal surface, and the amplitude of the wave is damped out in a skin depth d. A dc magnetic field is applied along the hard crystal direction in the basal plane, in a direction perpendicular to the polarization of the photon beam (which is taken to be in the $\hat{x}$ direction for this calculation). The spin system is assumed to be aligned fully along the applied field in the ground state.

Let $W_{\beta\beta'}$ = probability/time of transition from state β to β', where β and β' are states of the spin system. Then $W_{\beta\beta'} = \frac{2\pi}{\hbar} |<\beta'|V|\beta>|^2$ $\delta(E_\beta - E_{\beta'} + \hbar\omega)$ as is given by the "golden rule" for the absorption of quantum $\hbar\omega$ from a time-dependent electromagnetic perturbation field. We calculate $W_{\beta\beta'}$ for the photon-magnon interaction in an optical pumping experiment. The microwave magnetic field intensity inside the metal is:

$$\vec{H} = [H_0 e^{-z(1+i)/d} e^{i\omega t} + c.c.]\,\hat{x},$$

and the perturbation potential is:

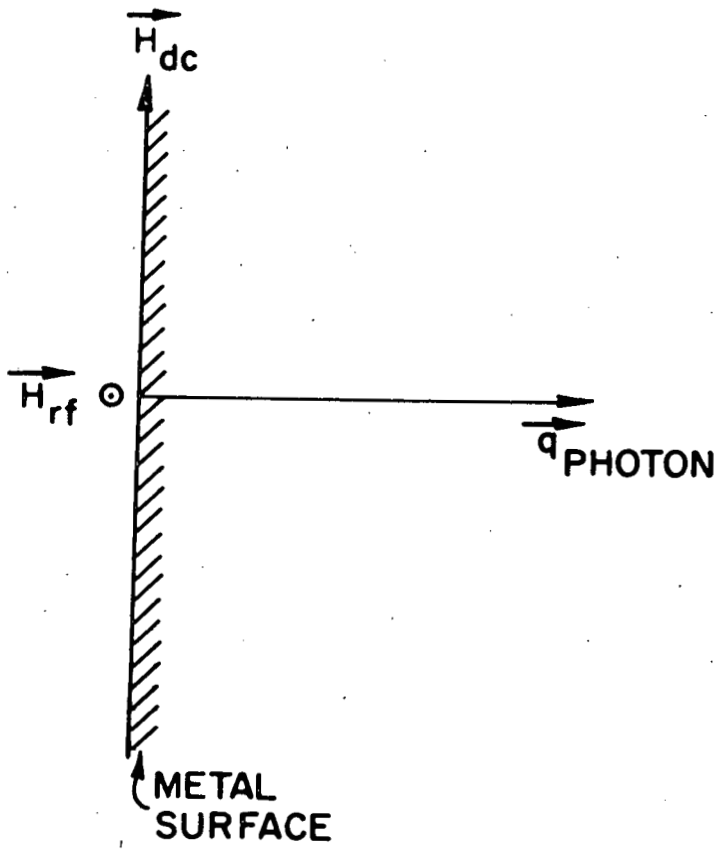

Figure 3. The geometry of a typical ferromagnetic resonance experiment. The crystal is cut so that the basal plane lies parallel to the metal surface

$$V(t) = -\sum_f \vec{\mu}_f \cdot \vec{H}(\vec{R}_f, t)$$

$$= -\sum_f [\mu_{fx} H_0 e^{-Z_f(1+i)/d} e^{i\omega t} + c.c.] .$$

Here $\vec{\mu}_f$ is the magnetic moment on the $f^{\underline{th}}$ site. We assume that other processes are more favorable to magnon decay than the photon-magnon interaction, so we only consider absorption processes. Therefore we omit the complex conjugate term and obtain:

$$V = -\sum_f [\mu_{fx} H_0 e^{-Z_f(1+i)/d}] .$$

Now

$$S_{fx} = -\frac{\mu_{fx}}{g\mu_B} = \frac{1}{2}(S_f^+ + S_f^-) = \sqrt{\frac{S}{2}}(a_f + a_f^\dagger) .$$

Here g is gyromagnetic ratio, μ_B is Bohr magneton, and a_f is a boson spin annihilation operator on the $f^{\underline{th}}$ site. Substitution of spin deviation operators for μ_{fx} yields:

$$V = \sqrt{\frac{S}{2}}\, g\mu_B H_0 \sum_f e^{-Z_f(1+i)/d} (a_f + a_f^\dagger).$$

Now Fourier transform the boson operators:

$$V = H_0 \sum_f \sum_{\vec{q}} e^{-Z_f(1+i)/d} [a_{\vec{q}}\, e^{-i\vec{q}\cdot\vec{R}_f} + a_{\vec{q}}^\dagger\, e^{i\vec{q}\cdot\vec{R}_f}] \sqrt{\frac{S}{2N}}\, g\mu_B .$$

Summing first over the X_f and Y_f components of $\vec{R}_f$, then over q_x and q_y we obtain:

$$V = \sqrt{\frac{SN}{2}}\, g\mu_B\, H_0 \sum_{Z_f} \sum_{q} e^{-Z_f(1 + i)/d} \left[a_q\, e^{-iq\, Z_f} + a_q^{\dagger}\, e^{iq\, Z_f}\right] \frac{1}{N_z} .$$

Here N_z is the number of unit cells in the z direction, and $N = N_x N_y N_z$. The suppressed notation $q_z \equiv q$ and $a_q \equiv a_{0,0,q}$ is also used.

Now the damping distance $d \ll L_z$ the thickness of the crystal. So one may take the upper limit of the sum on Z_f as ∞ with negligible error, and convert the sum to an integral:

$$\sum_{Z_f} \rightarrow \int_0^{\infty} \frac{dz}{c} ,$$

c being the hcp lattice parameter. Then using $N_z c = L_z$, we can write:

$$V = i\, H_0 \sqrt{\frac{SN}{2}}\, \frac{g\mu_B}{L_z} \sum_{q} \left[\frac{a_q}{(q + \frac{1}{d} - \frac{i}{d})} + \frac{a_q^{\dagger}}{(\frac{1}{d} - q - \frac{i}{d})}\right] . \qquad (12)$$

Now we make a Bogoliubov transformation from the boson operators a_q to the magnon operators α_q:

$$a_q = u_q \alpha_q - v_q \alpha_{-q}^{\dagger} . \qquad (13)$$

Here u_q and v_q are c-numbers and satisfy:

$$u_q^{*} = u_{-q} = u_q ,$$

$$v_q^{*} = v_{-q} = v_q .$$

Substitution of Equation (13) into the commutation relation $[a_q, a_q^{\dagger}] = 1$, and requirement that α_q satisfy the boson commutation rules gives the relation:

$$u_q u_q^* - v_q v_q^* = 1 \quad . \tag{14}$$

The requirement that the Hamiltonian of Equation (10) be diagonal in α_q:

$$H_m = \sum_q E(q)\, \alpha_q^\dagger \alpha_q \quad ,$$

with

$$E(q) = [(A_q)^2 - (B_q)^2]^{1/2} \quad ,$$

gives further relations among the c-numbers:

$$u_q u_q^* + v_q v_q^* = A_q/E(q) \quad ,$$

$$2u_q v_q = B_q/E(q) \quad . \tag{15}$$

Then under the transformation of Equation (13), Equation (12) becomes:

$$V = iH_o (SN/2)^{1/2} g\mu_B/L_z \sum_q [(u_q^* - v_{-q})(-q + 1/d - i/d)^{-1} \alpha_q^\dagger$$

$$+ (u_q - v_{-q}^*)(q + 1/d - i/d)^{-1} \alpha_q] \quad .$$

Using the Equations (14) and (15), the square of the matrix element for the absorption of one photon, and the creation of one magnon of wavenumber q is:

$$|\langle n_q + 1|V|n_q\rangle|^2 = |H_0|^2 \frac{SN}{2} \frac{g^2\mu_B^2}{L_z^2} \frac{(n_q + 1)}{[(\frac{1}{d} - q)^2 + \frac{1}{d^2}]\ (A_q + B_q)} \quad .$$

Here $n_q = [e^{\beta E(q)} - 1]^{-1}$, and $E(q) = (E_{\beta'} - E_\beta)$ is the magnon energy with wavevector q. We assume that $n_q \approx \frac{kT}{E(q)} \gg 1$ in all regions of temperature and wavevector of interest. Then the transition probability $W_{(q)}$ is

given by:

$$W_{\omega}(q) = \frac{NS\pi}{\hbar} \frac{g^2\mu_B^2}{L_z^2} |H_0|^2 \frac{kT}{(A_q + B_q)} \frac{\delta[\hbar\omega - E(q)]}{(\frac{1}{d} - q)^2 + \frac{1}{d}2} \quad . \qquad (16)$$

Neutron diffraction studies show that the magnon spectrum is broadened somewhat at q = 0, so we will assume a Lorentzian broadening of the energy at fixed wavevector. To account for this in Equation (16) we make the replacement:

$$\delta[\hbar\omega - E(q)] \rightarrow \frac{\gamma_m/\pi}{[\hbar\omega - E(q)]^2 + \gamma_m^2/4} \quad .$$

Here γ_m is the width of the magnon spectrum. Since $\vec{H}$ is parallel to the metal surface, it is continuous across it. Thus H_0 is the amplitude of the incident radiation, and $|H_0|^2$ is related to the element of area under the intensity distribution of the photons in the following way:

$$S_{av} = I(\omega)\, d\omega = \frac{c_0}{8\pi} \mathrm{Re}(\vec{E} \times \vec{B}^*) = \frac{c_0}{8\pi} |H_0|^2 \quad .$$

Here $\vec{S}_{av}$ is the time-averaged Poynting vector at the metal surface, and c_0 is the speed of light. Thus:

$$|H_0|^2 = \frac{8\pi}{c_0} I(\omega) d\omega \quad .$$

Now assume a Lorentzian shape for the photon spectrum:

$$I(\omega) = \frac{\gamma_{ph}}{\pi} [(\omega - \bar{\omega}_{rf})^2 + \gamma_{ph}^2/4]^{-1} \quad .$$

Here γ_{ph} is the width of the spectrum and $\bar{\omega}_{rf}$ is the center frequency of

the incident radiation. Making the above replacements and substitutions in Equation (16) and integrating over all photon frequencies we obtain:

$$W(q) = \frac{NS\pi g^2 \mu_B^2}{\hbar^2 L_z^2 c_0} \frac{kT}{(A_q + B_q)} \left[\left(\frac{1}{d} - q\right)^2 + \frac{1}{d^2}\right]^{-1} \frac{(\gamma_{ph} + \gamma_m)}{\pi}$$

$$\left\{\left[\bar{\omega}_{rf} - E(q)/\hbar\right]^2 + (\gamma_{ph} + \gamma_m)^2/4\right\}^{-1}.$$

The photon beam is usually generated in a klystron tube and has a narrow linewidth. So we assume $\gamma_m \gg \gamma_{ph}$. Then the transition rate from state with n_q magnons to $n_q + 1$ magnons becomes:

$$W(q) = \frac{N_0 kT}{L_z (A_q + B_q)} \left\{\frac{\gamma_m^2}{4} + \left[\bar{\omega}_{rf} - E(q)/\hbar\right]^2\right\}^{-1} \left[\frac{1}{d^2} + \left(\frac{1}{d} - q\right)^2\right]^{-1} .$$

Here $N_0 = \dfrac{8NS\, g^2 \mu_B^2 \pi \gamma_m}{c_0 L_z \hbar^2}$ and is independent of L_z by virtue of N in the numerator.

The transition rate to the q = 0 state is then:

$$W(0) = \frac{N_0 kT d^2}{(A_o + B_o) L_z} \left\{\frac{\gamma_m^2}{4} + \left[\bar{\omega}_{rf} - E(0)/\hbar\right]^2\right\}^{-1} . \qquad (17)$$

The total transition rate to the states $q \neq 0$ is given by:

$$W_T = \frac{L_z}{2\pi} \int_{0^+}^{\pi/c} dq W(q) = \frac{N_0 kT}{2\pi} I_{d'} \qquad (18)$$

where

$$I_d = \int_{0^+}^{\pi/c} \frac{dq}{(A_q + B_q)} \left\{ \frac{\gamma_m^2}{4} + [\bar{\omega}_{rf} - E(q)/\hbar]^2 \right\}^{-1} \left[\frac{1}{d^2} + \left(\frac{1}{d} - q \right)^2 \right]^{-1} .$$

Equation (18) represents the total absorption by frozen lattice magnons; whereas, Equation (17) is only proportional to the absorption by free lattice magnons. To obtain the total contribution one must multiply Equation (17) by the number of free lattice states. Using the formula for the skin depth of periodic crystal distortion derived by Evenson and Liu (5), one can estimate the number of such states. Taking the radiation skin depth of the metal to be 10^4 Å, clamping is found to be ineffective within this skin depth for magnons of wavenumber less than 10^{-4} Å^{-1}. This corresponds to about 10^3 magnon states along the hexagonal axis of the Brillioun zone of Tb or Dy metal (using sample dimensions typical of published FMR work). The total absorption by free lattice magnons is then $W_T' = 10^3 W(0)$. The integral I_d was computed numerically, and $E(q) = E(0^+) + Cq^2$ was assumed in the integration. The microwave absorption versus external field is plotted for a variety of temperatures in Figures 4 through 8 for Dy and Tb. These absorption curves were normalized by taking the maximum absorption at each temperature equal to unity. The curves are drawn only for field values above the domain alignment field (i.e., that field necessary to align all the magnetic moments ferromagnetically). Such a domain alignment field is finite even below the Curie temperature since ferromagnetically aligned domains tend to align in a random fashion along the three easy axes in the basal plane.

The absorption of 10 GHz microwaves is shown in Figure 4 for Dy metal. The absorption profile below the Curie point (85 K) is characterized by a sharp rise, followed by a long asymmetric tail which persists to very high field values. Virtually all the absorption in the peak region is due to free lattice magnon processes. The ratio, W_T/W_T' is less than 0.2 near the peak at the three temperatures shown. Absorption profiles above the Curie temperature have the same characteristics as the 90 K curve shown in the Figure. In this curve the strongest microwave absorption occurs at the "critical field", that field at which the antiferromagnetically aligned domains flip into a fan or ferromagnetic configuration. Thus, in the high temperature region, the spin wave absorption is masked by strong domain alignment effects. The long tail in the observed absorption (20) is due to off-resonance absorption by both free and frozen lattice states, the frozen lattice states contributing most strongly. At 150 K, for example, the ratio W_T/W_T' is 4.5 over the whole field sweep. One should note a tendency for the linewidth of the absorption to narrow with increasing temperature below the Curie point. This tendency was observed by Bagguley (16), and later by Rossol (17).

The absorption of 20 GHz microwaves is shown in Figure 5 for Tb metal. The general characteristics of the absorption are the same as for Dy. At low temperatures there is a rather sharp high field peak. The position of this peak shifts to lower fields as temperature increases, until it falls below the domain alignment field at 140 K. The maximum in the absorption is again masked at high temperatures by domain alignment

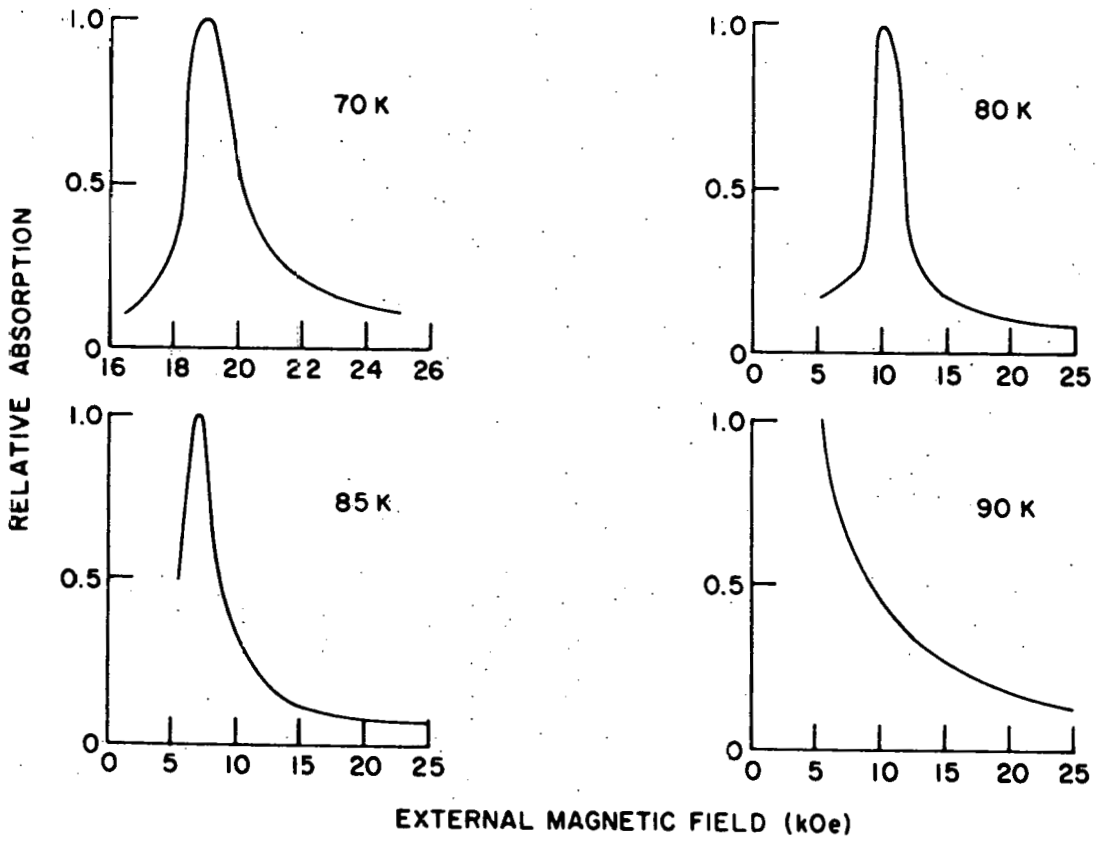

Figure 4. Microwave absorption versus external field in Dy metal at 10 GHz

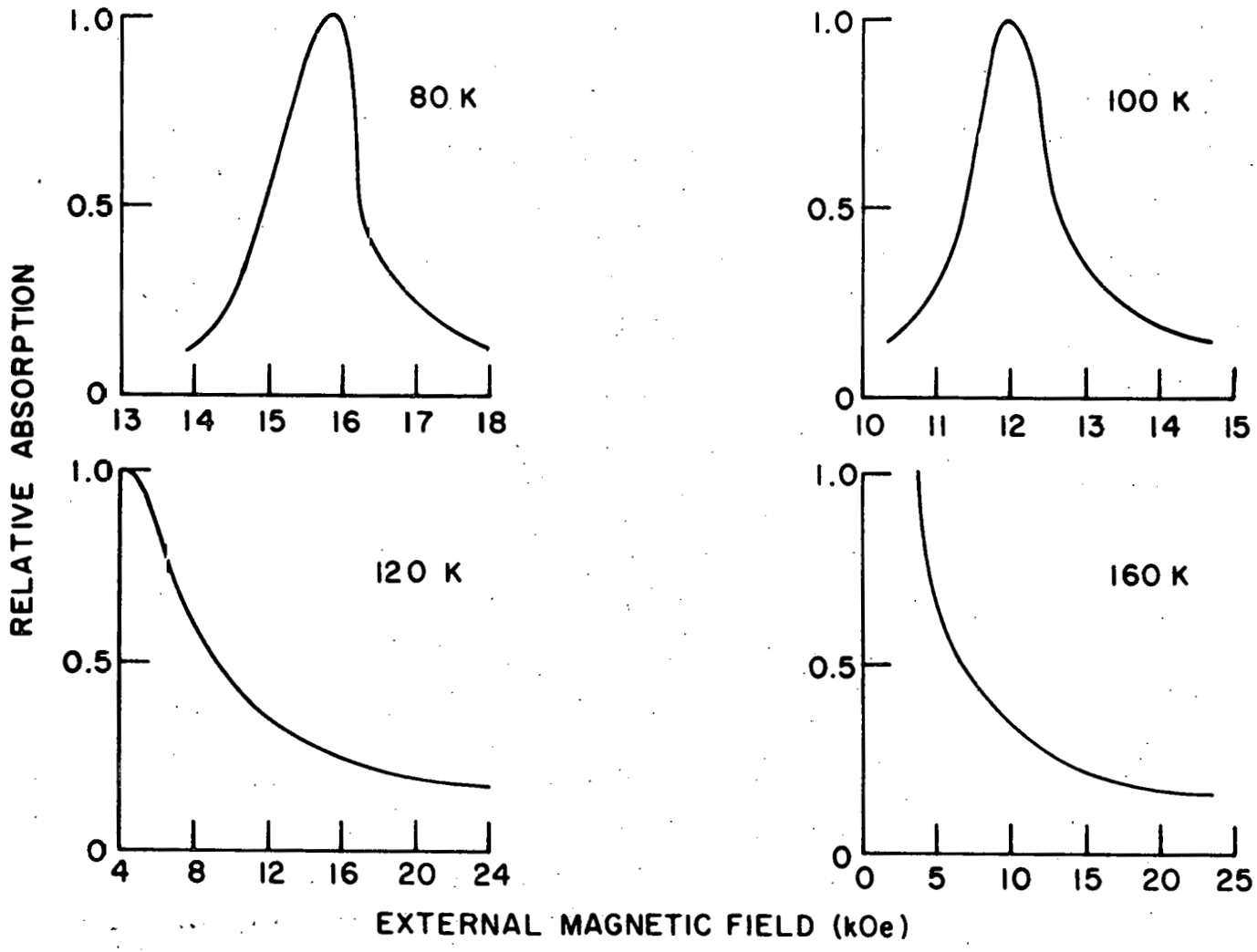

Figure 5. Microwave absorption versus external field in Tb metal at 20 GHz

effects, but the long tail should still be observable, and is due primarily to off-resonance absorption by the frozen lattice states. The absorption below 120 K is due mainly to free lattice magnon processes, W_T/W'_T being less than 0.2 in the peak region. This ratio increases to about 1.0 at 140 K, and frozen lattice magnon processes dominate the absorption above 160 K. The characteristics of the absorption profiles shown in Figures 4 and 5 (i.e., general shape and peak positions) are observed experimentally (16,20,21).

The absorption of 40 GHz radiation below the Curie temperature is shown versus field in Figure 6. A barely resolvable double peak occurs below 85 K. Experimentally the double peak is not observed (17), a fact which is not surprising because the peaks are so close, overlapping almost entirely. A strong single peak is observed, however, and occurs near the center of the calculated double peak (17). The ratio W_T/W'_T is about 0.2 in the peak region, so that on-resonance absorption by free lattice states is the important absorption mechanism in the production of the peak.

The absorption of 100 GHz radiation in ferromagnetic Tb is shown in Figure 7. Below 200 K, the primary absorption occurs at the domain alignment field due to the sharp low field dip in the frozen lattice magnon gap (see Figure 2) which makes the off-resonance absorption by frozen lattice states quite strong. At higher fields in the low temperature region, weak structure appears due to on-resonance absorption by free lattice magnons. This structure, however, is not resolvable experimentally (17) probably because of the especially low sensitivity of high frequency microwave experiments. This weak absorption structure is also masked by the

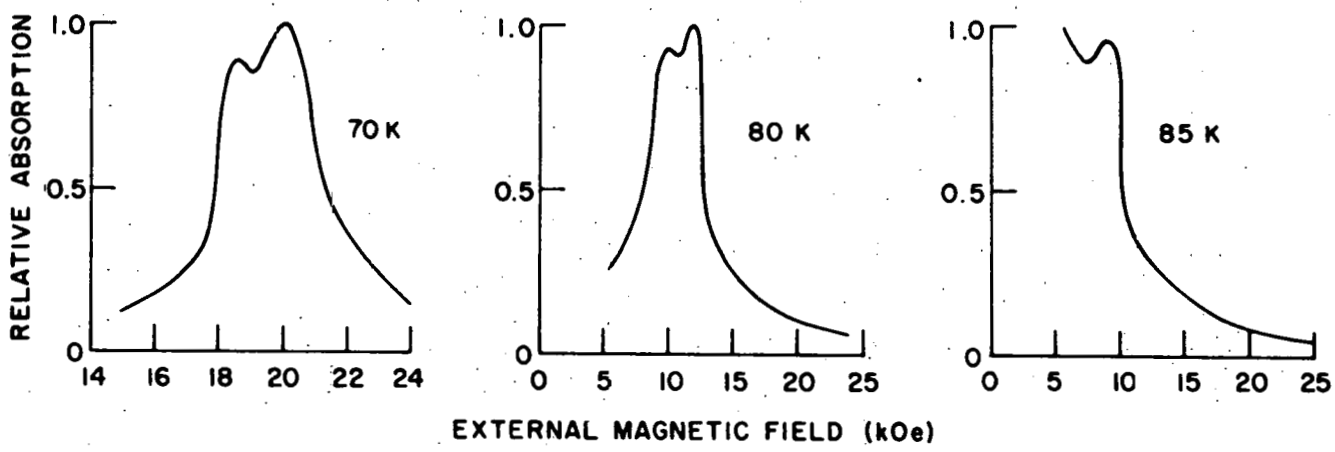

Figure 6. Microwave absorption versus external field in Dy metal at 40 GHz

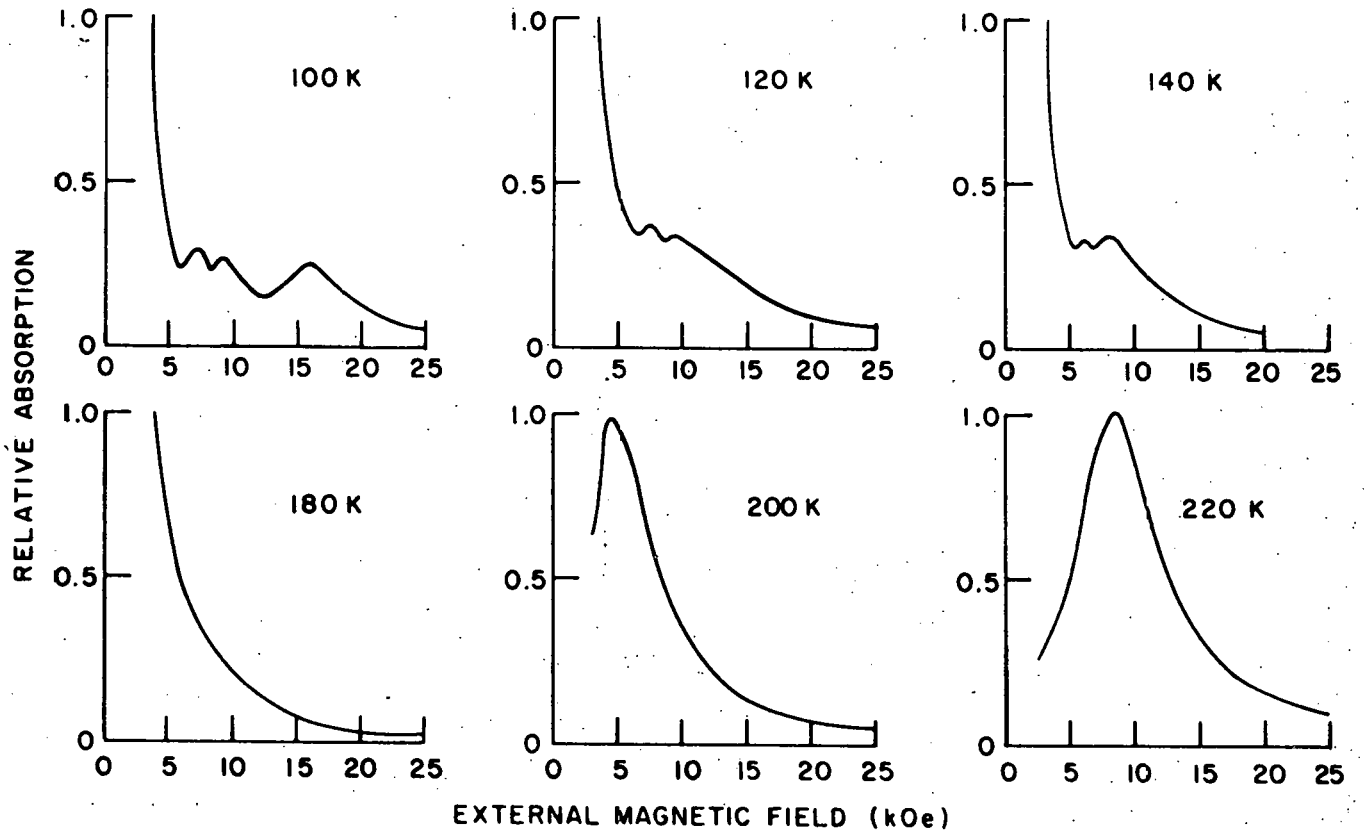

Figure 7. Microwave absorption versus external field in Tb metal at 100 GHz

very strong absorption near domain alignment. Above 200 K, on-resonance absorption by the frozen lattice states becomes possible. The field at which this resonance occurs increases with increasing temperature, shifting the peak to higher fields.

The absorption of 100 GHz radiation for Dy metal is shown in Figure 8. A strong double peak appears below 80 K, and is due almost entirely to on-resonance absorption by free lattice states. Above 85 K, the low field peak is lost below the domain alignment field; and at 110 K the high field peak is lost. The curve shown at 110 K is representative of curves at higher temperatures. In this curve maximum absorption occurs at the critical field, and is followed by a long absorption tail. Off-resonance frozen lattice processes are responsible for most of this absorption. The profiles shown in Figure 8 have been observed in Dy for temperatures above the Curie temperature (35). According to our calculation, the double peak should be clearly observable at 70 K, although no accurate study of ferromagnetic Dy has been made to date. Future observation of this double peak would substantiate further the evidence that free lattice magnons play an important role in low temperature microwave absorption.

The resonance field is defined as that field at which maximum absorption occurs. The resonance field versus temperature for Dy metal is shown in Figure 9 for microwave frequencies of 40 GHz and 100 GHz along with experimental points (17,35). The theoretical curves are obtained by taking the field values at which the calculated microwave absorption is a maximum. The average position is taken in the case of barely

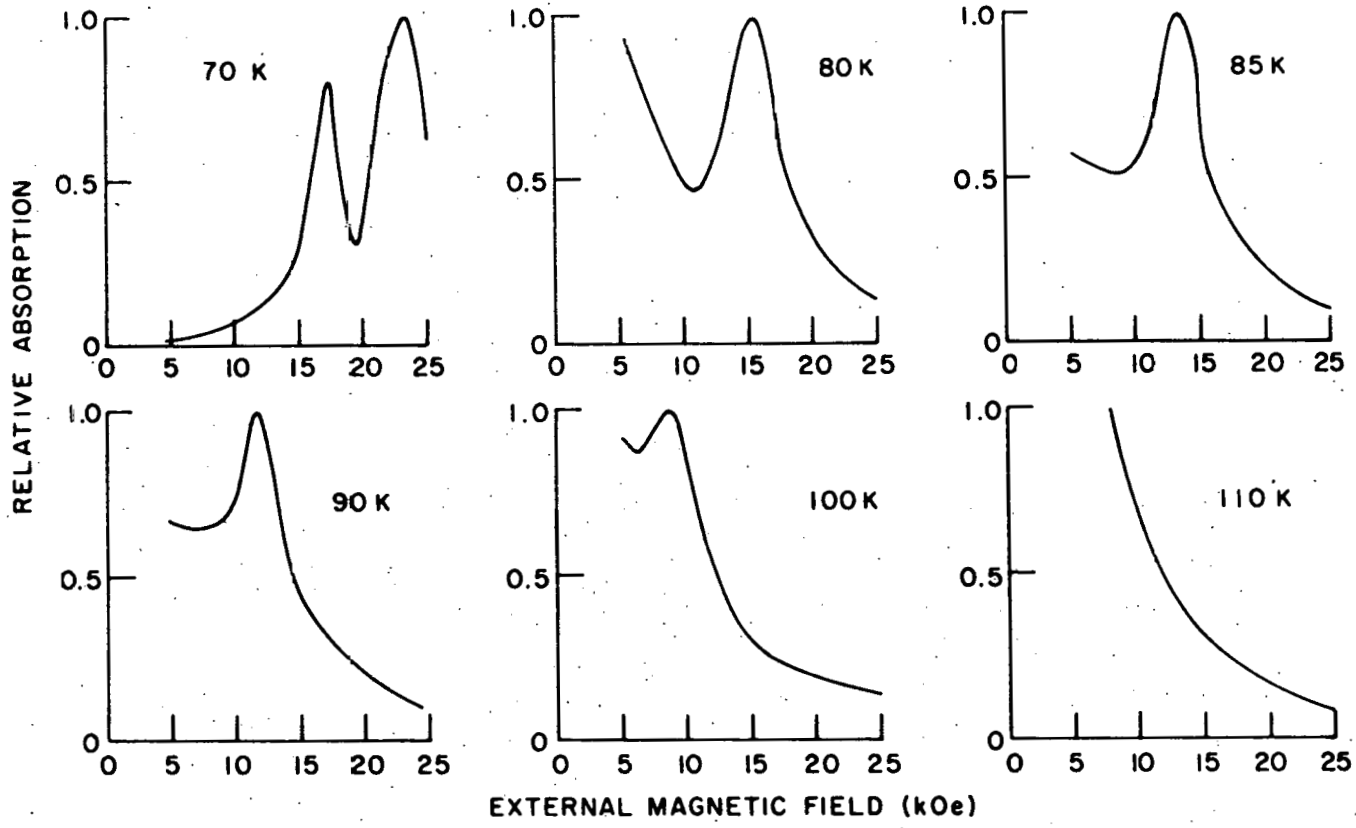

Figure 8. Microwave absorption versus external field in Dy metal at 100 GHz

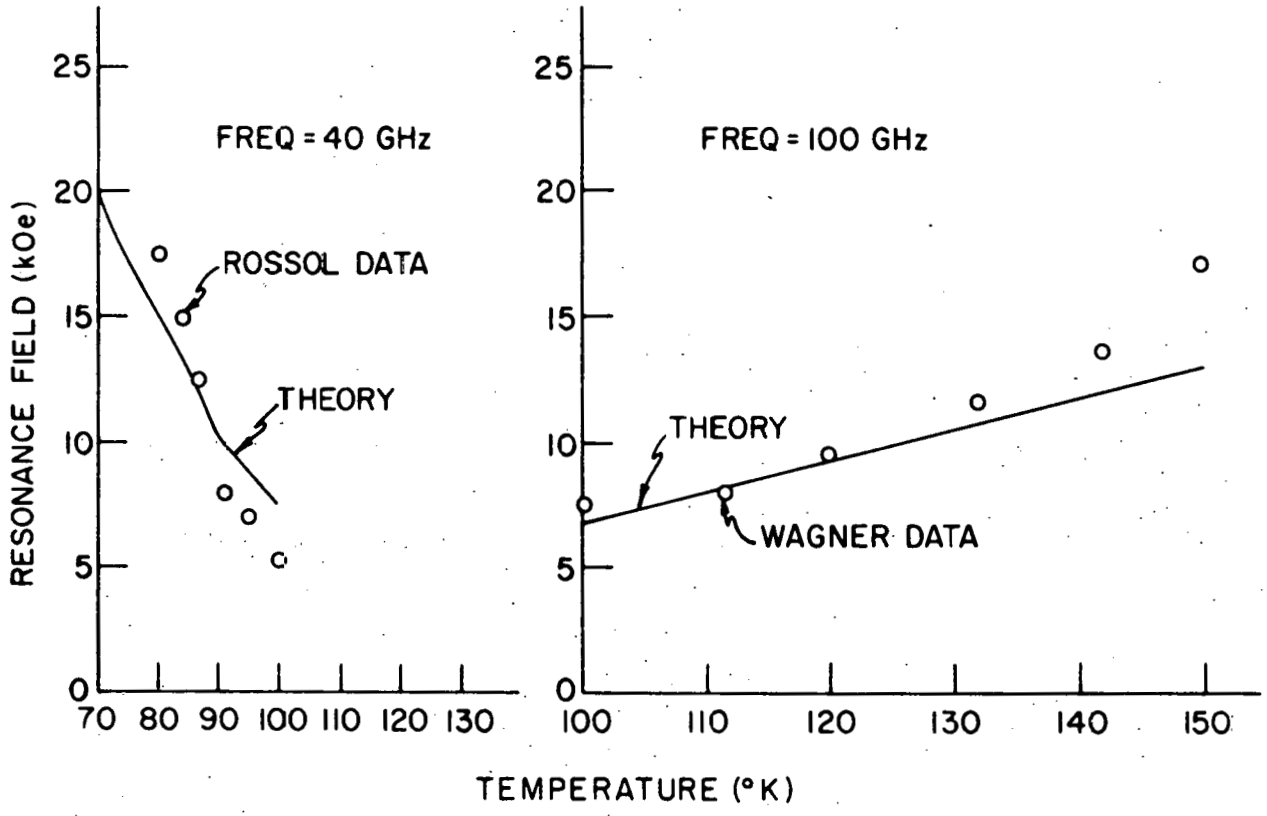

Figure 9. Resonance field versus temperature for dysprosium metal

resolvable double peaks. At 40 GHz, the resonance field increases dramatically as temperature is reduced in the ferromagnetic regime. This is due to the on-resonance absorption by free lattice magnons, which occurs most strongly near the planar anisotropy field where E(0) dips to zero (see Figure 1). The planar anisotropy field increases with decreasing temperature, producing the sharp rise in the resonance field. The data of Rossol verify this predicted rise quite conclusively. Above the Curie temperature, the 100 GHz absorption peaks occur at the critical field so that the data of Wagner follows the critical field curve quite well, except for a small deviation toward higher fields above 140 K.

Below the Curie temperature of Dy free lattice magnon absorption is the dominant process at both 40 GHz and 100 GHz. Above the Curie temperature, frozen lattice absorption is the dominant process at both 40 GHz and 100 GHz. Thus, one expects the temperature dependence of the resonance field to be similar at both 40 GHz and 100 GHz over the complete ordered regime of Dy. In ferromagnetic Tb, below 140 K, frozen lattice magnon processes dominate 100 GHz absorption producing a peak at the domain alignment field; whereas, free lattice magnon processes dominate 20 GHz absorption producing a peak at the effective planar anisotropy field. Therefore, the theory predicts a striking difference in the behavior of the resonance field curves at the two frequencies. The resonance field versus temperature for Tb metal at 20 GHz and at 100 GHz is shown in Figure 10 along with the experimental points (21,19). There is a dramatic increase of 8kOe in the 20 GHz curve between 140 K and 100 K. Over the

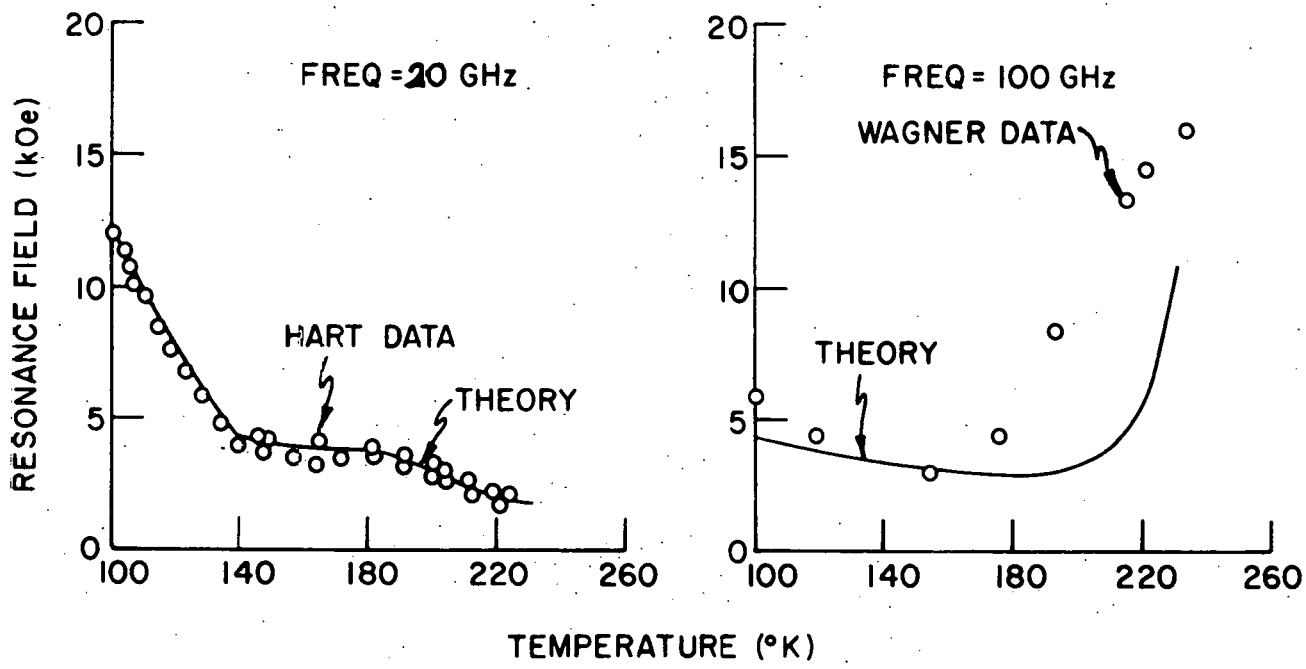

Figure 10. Resonance field versus temperature in Tb metal

same temperature interval, the 100 GHz curve changes less than 1kOe. The experimental points fall almost exactly on the theoretical curves, providing an extremely strong confirmation of the theory.

One notes that good experimental agreement is attained in both metals using the statically measured planar anisotropy constants with a temperature renormalization of $\hat{I}_{13/2}$ for Dy and $\hat{I}_{9/2}$ $\hat{I}_{5/2}$ for Tb. A neutron diffraction study of Tb (5) has verified that the planar anisotropy of that metal is of magnetoelastic origin, so that the temperature renormalization $\hat{I}_{9/2}$ $\hat{I}_{5/2}$ is well justified. The renormalization $\hat{I}_{13/2}$ for Dy assumes that the planar anisotropy arises from crystal field symmetry in this metal. Such an assumption seems to be well justified by the excellent agreement of the theory with microwave absorption data. A neutron diffraction study of Dy, similar to that done for Tb, seems appropriate at this time to see if there is indeed a difference in the origin of the planar anisotropy in these metals. The microwave experiments point very strongly to this conclusion.

THE MAGNON-PHONON INTERACTION

In the preceding chapter we computed the effects of uniform magnetostriction on the spin wave energies. In this chapter, we calculate the effect of arbitrary vibrations of the crystal ions about the uniformly strained configuration produced by the spin order. In general, the vibrations produce non-uniform strains which couple locally to the spin system through the local magnetoelastic interaction of Evenson and Liu [see Equation (6)]. Normal modes of lattice and spin vibrations couple strongly when vibrational frequencies are nearly equal, producing mixed spin-lattice modes (36).

Figure 11 shows the experimental magnon and phonon dispersion curves along the c-axis of pure Tb metal at 79 K in the reduced zone scheme (37). The dashed lines indicate the dispersion curves expected without spin-lattice coupling. The solid lines are drawn through the experimental points. In the region where the transverse optical phonon branch (TO) crosses the acoustical magnon branch (MA), a large splitting, labelled Δ_2, is observed. In the region where the transverse acoustical phonon branch (TA) "kisses" the acoustical magnon branch (MA), a smaller splitting, Δ_1, is observed. The magnetoelastic coupling removes the degeneracy of the spin and lattice modes, and the size of the branch splitting is a measure of the coupling strength. The states in the region of strong spin-lattice coupling are magnon-phonon quasi-particle states. It is the purpose of this chapter to calculate the splittings expected on the basis of Equation (6).

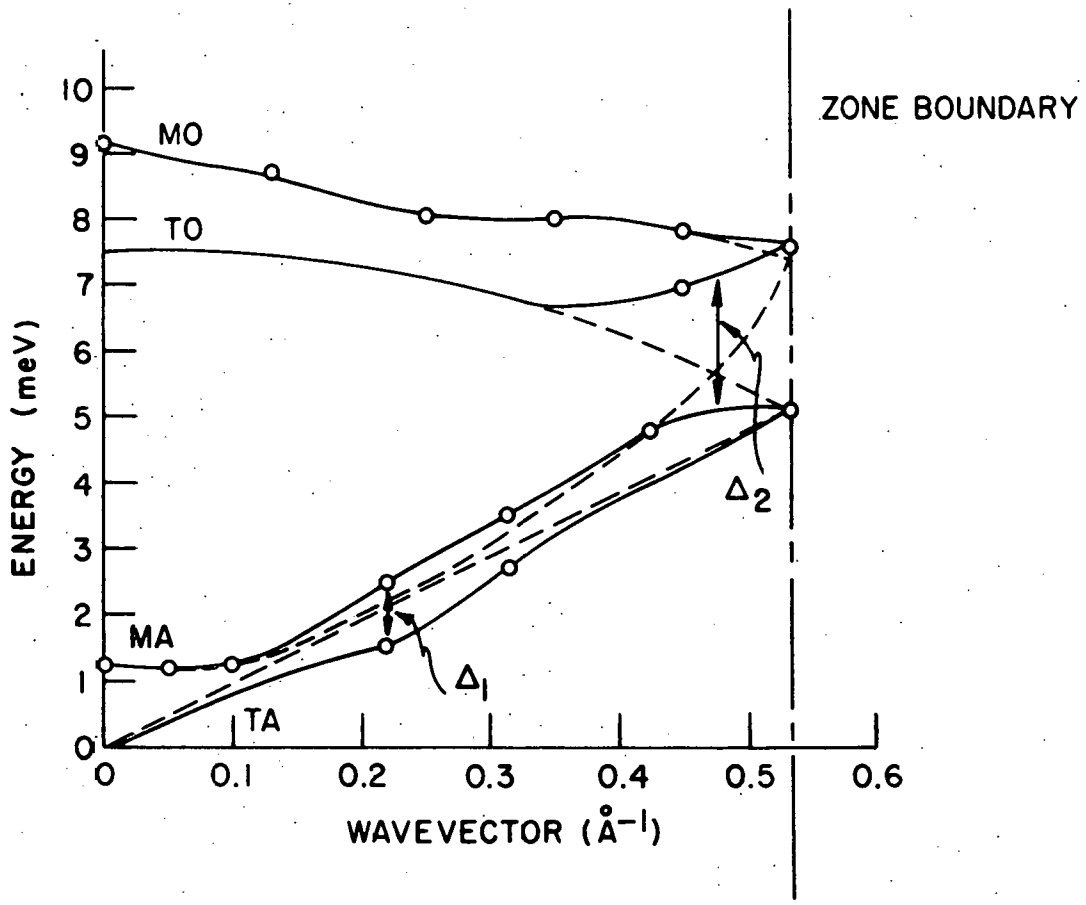

Figure 11. The magnon (MA, MO) and transverse phonon (TA, TO) dispersion curves for terbium in the c-direction at 79 K. The magnon-phonon interaction causes a mixing of modes and splittings at the crossing points of the unperturbed dispersion curves (indicated by dashed lines)

First we compute the ϵ-representation terms of the magnetoelastic interaction. The local strain functions for this representation are:

$$\mathcal{E}^{\epsilon}_{1f} = \frac{1}{2} \sum_{\delta} [\, \delta_x \, (r_f{}^z - r_{f+\delta}{}^z) + \delta_z \, (r_f{}^x - r_{f+\delta}{}^x)],$$

$$\mathcal{E}^{\epsilon}_{2f} = \frac{1}{2} \sum_{\delta} [\, \delta_y \, (r_f{}^z - r_{f+\delta}{}^z) + \delta_z \, (r_f{}^y - r_{f+\delta}{}^y)] \, . \tag{19}$$

Here $f = (\ell, s)$ labels the position of the $f^{\underline{th}}$ atom in the crystal, and δ labels the positions of its twelve nearest neighbors.

From lattice vibration theory, the second quantized form of the components of displacement from the unstrained equilibrium positions is given by:

$$r^{i}_{\ell s} = \sum_{\rho, \vec{q}} R_{\rho, \vec{q}} \; V^{\vec{q}\rho}_{is} \; e^{i\vec{q}\cdot\vec{\ell}} \; (\beta_{-\vec{q}\rho}{}^{\dagger} + \beta_{\vec{q}\rho}) \, . \tag{20}$$

Here $i = (x, y, z)$, and $s = (0, c/2)$ labels the two atoms of the unit cell; ρ labels the mode of vibration, and ℓ labels the unit cell. The quantity $R_{\rho\vec{q}} = (\hbar/Nm\, \omega_{\rho\vec{q}})^{1/2}$, where N is the number of unit cells, m is the mass of an ion, and $\omega_{\rho\vec{q}}$ is the frequency of a normal mode of crystal vibration. The quantities $v^{\vec{q}\rho}_{is}$ are the components of the polarization vector of the lattice wave, and β and β^{+} are the annihilation and creation operators for the phonons. The components of the polarization vector must satisfy the following orthonormality condition:

$$\sum_{i,s} (v^{\vec{q}\rho}_{is})^{*} \quad (v^{\vec{q}\rho'}_{is}) = \delta_{\rho\rho'} \, . \tag{21}$$

In order to compare the results of the calculation with measurements on Tb, we assume the lattice modes to be propagating along the $\hat{c}$-axis of a hcp crystal, and to be transverse polarized along the $\hat{a}$-axis in the basal plane. The Cartesian coordinates appearing in Equations (19) are defined with $\hat{x}$ along $\hat{a}$ and $\hat{z}$ along $\hat{c}$. For such lattice waves, the solution to Equation (21) for the polarization vectors is:

$$v_{x0}^{q\rho} = \frac{1}{\sqrt{2}}\ \hat{a}\ , \quad (\rho = 1,2)\ ,$$

$$v_{x\,c/2}^{q1} = \frac{1}{\sqrt{2}}\ e^{iq\,c/2}\ \hat{a}\ ,$$

$$v_{x\,c/2}^{q2} = \frac{-1}{\sqrt{2}}\ e^{iq\,c/2}\ \hat{a}\ ,$$

$$v_{ys}^{q\rho} = v_{zs}^{q\rho} = 0\ . \quad (s = 0,\ c/2;\ \rho = 1,2) \tag{22}$$

Then, using Equations (22) in Equation (20), we find the local strains of Equations (19) to be:

$$\varepsilon_{1f}^{\ \epsilon} = \frac{3ic}{2\sqrt{2}} \sum_{q,\rho} R_{\rho\vec{q}}\ e^{i\vec{q}\cdot\vec{f}} \sin\frac{qc}{2}\ (\beta_{-q\rho}^{\ \dagger} + \beta_{q\rho})\ \eta_{f\rho},$$

$$\varepsilon_{2f}^{\ \epsilon} = 0\ . \tag{23}$$

where

$$\eta_{f1} = \eta_{f2} = 1 \quad \text{if } f = (\ell, 0);\ \text{and } \eta_{f1} = -\eta_{f2} = 1 \quad \text{if } f = (\ell, c/2).$$

The summation on q is taken along the c-axis of the Brillioun zone in the single zone scheme. The hcp structure is considered to be made of two identical interpenetrating hexagonal sublattices. Two kinds of spin deviation operators, a_f and b_f are introduced corresponding to each of the two sublattices (38). Then the spin functions of the ϵ-representation are transformed to spin deviation operators as follows:

$$S_{lf}^{\epsilon} = -\sqrt{\frac{S^3}{2}} \quad (a_f^{\dagger} + a_f) \qquad f = (\ell, 0)$$

$$= -\sqrt{\frac{S^3}{2}} \quad (b_f^{\dagger} + b_f) \qquad f = (\ell, c/2) \quad . \tag{24}$$

Using Equations (23) and (24) in the local magnetoelastic Hamiltonian of Equation (6) and summing over lattice sites we obtain:

$$H_{me}^{\epsilon} = -\frac{\tilde{B}^{\epsilon}\sqrt{NS^3}}{2\sqrt{2}\ c} i \sum_{\rho q} R_{\rho q} \sin\frac{qc}{2} (\beta_{-q\rho}^{\dagger} + \beta_{q\rho}) [a_q^{\dagger} + a_{-q} + \lambda_{\rho}$$

$$(b_q^{\dagger} + b_{-q})] \ , \tag{25}$$

where $\lambda_{\rho} = 1$ if $\rho = 1$; and $\lambda_{\rho} = -1$ if $\rho = 2$.

Here a_q and b_q are the Fourier transforms of the spin deviation operators a_f and b_f.

The terms in the magnetoelastic Hamiltonian that transform according to the γ and α representations are calculated in an exactly similar way. A surprising result is that $H_{me}^{\gamma} = 0$. The local strains are zero in this case, due to the choice $\vec{q} = q\hat{c}$ and the hcp symmetry of the crystal. The

spin functions of the α representation all involve bilinear combinations of the magnon operators, so H_{me}^{α} contains only processes that do not conserve particle number, and which contribute only to broadening effects. A time dependent perturbation calculation was done to determine the amount of broadening caused by third order processes in the magnetoelastic Hamiltonian. In the mixed-mode region, the Tb spectrum was found to be broadened by 0.04 meV by the magnetoelastic interaction. This is quite small compared to the broadening caused by magnon-magnon processes in this part of the Brillioun zone.

Let H_{m-p} denote the total second-quantized Hamiltonian relevant to mode-mixing:

$$H_{m-p} = \frac{1}{2} \sum_{qj\rho} \{A_{qj}(a_q^{\dagger}a_q + b_q^{\dagger}b_q) + \frac{1}{2} B_{qj} (a_q^{\dagger}a_{-q}^{\dagger} + a_q a_{-q} + b_q^{\dagger}b_{-q}^{\dagger}$$

$$+ b_q b_{-q}) + \hbar\omega_{q\rho} \beta_{q\rho}^{\dagger}\beta_{q\rho} + \Delta_{q\rho} (\beta_{-q\rho}^{\dagger} + \beta_{q\rho})$$

$$[(a_q^{\dagger} + a_{-q}) + \lambda_{\rho} (b_q^{\dagger} + b_{-q})]\} , \qquad (26)$$

where

$$\Delta_{q\rho} = - \frac{\tilde{B} \epsilon \sqrt{NS^3}\, i}{2\sqrt{2}\, c} \sin \frac{qc}{2} R_{\rho q} .$$

The quantity $\hbar\omega_{\rho q}$ is the unperturbed phonon energy, and A_{qj} and B_{qj} are the coefficients that appear in Equation (10) with a subscript $j = 1,2$ added to denote acoustical or optical magnon branches respectively. (The earlier discussion was in the double zone scheme using a Bravais lattice.)

The factor 1/2 in Equation (26) is inserted to prevent double counting. The boson operators a_q and b_q are a mixture of acoustical and optical magnon annihilation operators. We define operators c_q and d_q by the following transformation:

$$a_q = \frac{1}{\sqrt{2}} \quad (c_q + d_q) \quad ,$$

$$b_q = \frac{1}{\sqrt{2}} \quad (c_q - d_q) \quad . \tag{27}$$

Expressing H_{m-p} in terms of these new boson operators we obtain:

$$H_{m-p} = \frac{1}{2} \sum_{qj\rho} \{ A_{qj} \ (c_q^{\dagger} c_q + d_q^{\dagger} d_q) + \frac{1}{2} \ B_{qj} \ (c_q^{\dagger} c_{-q}^{\dagger} + c_q c_{-q} + d_q^{\dagger} d_{-q}^{\dagger}$$

$$+ d_q d_{-q}) + \hbar\omega_{\rho q} \ \beta_{q\rho}^{\dagger} \beta_{q\rho} + \sqrt{2} \Delta_{q\rho} \ (\beta_{-q\rho}^{\dagger} + \beta_{q\rho})$$

$$[(c_q^{\dagger} + c_{-q}) \ \delta_{\rho 1} + (d_q^{\dagger} + d_{-q}) \ \delta_{\rho 2}] \ \} \quad . \tag{28}$$

Here $\delta_{\rho 1}$ and $\delta_{\rho 2}$ are Kronecker deltas. Finally, we make a Bogoliubov transformation of the operators c_q and d_q to magnon creation and annihilation operators:

$$c_q = u_{1q} \alpha_{1q} - v_{1q} \alpha_{1,-q}^{\dagger} \quad ,$$

$$d_q = u_{2q} \alpha_{2q} - v_{2q} \alpha_{2,-q}^{\dagger} \quad . \tag{29}$$

Here α_{1q} and α_{2q} are the annihilation operators for acoustical and optical

magnons respectively. The coefficients of the transformation satisfy relations analogous to Equations (15). Substitution of Equations (29) into Equation (28) yields:

$$H_{m-p} = \sum_{j,q} E_j(q)\, \alpha_{jq}^{\dagger} \alpha_{jq} + \sum_{\rho,q} \hbar\omega_{\rho q}\, \beta_{q\rho}^{\dagger} \beta_{q\rho}$$

$$+ \sum_{j\rho q} \left[\frac{E_j(q)}{2(A_{qj} + B_{qj})} \right]^{-1/2} \Delta_{q\rho}\, \delta_{j\rho}\, (\alpha_{jq}^{\dagger} + \alpha_{j,-q})(\beta_{\rho,-q}^{\dagger} + \beta_{\rho q}) \,. \qquad (30)$$

By virtue of the Kronecker delta $\delta_{j\rho}$ that appears in Equation (30), the magnetoelastic interaction of Evenson and Liu, Equation (6), fails to account for the coupling of acoustical and optical modes. This interaction was originally devised in order to describe static effects, and so couples only local displacements to the spin system. In the excited states of the lattice, however, dynamic quantities, such as lattice angular momentum, may couple to the spins. In the Appendix, it is shown that a kind of "L-S coupling" does in fact couple the acoustical magnons to the optical phonons, giving rise to a splitting. This mechanism, however, does not lead to any coupling of acoustical modes, so let us use the mode-mixing Hamiltonian H_{m-p} to calculate the splitting between the TA and MA branches shown in Figure 11.

For the mixing of these specific modes H_{m-p} reduces to:

$$H_{m-p} = \sum_{q} E(q)\, \alpha_q^{\dagger} \alpha_q + \sum_{q} \hbar\omega_q\, \beta_q^{\dagger} \beta_q$$

$$+ \sum_{q} \Delta_q' \, (\alpha_q^{\dagger} + \alpha_{-q})(\beta_{-q}^{\dagger} + \beta_q) \,. \qquad (31)$$

Here $\Delta_q' = \left[\frac{E(q)}{2(A_q + B_q)}\right]^{-1/2} \Delta_q$, and the mode labels ρ and j are suppressed. We diagonalize this Hamiltonian by defining a new annihilation operator:

$$\gamma_q = t_1 \alpha_{-q} + t_2 \alpha_q^{\dagger} + t_3 \beta_{-q} + t_4 \beta_q^{\dagger} .$$

The imposition of the condition $[\gamma_q, H_{m-p}] = \Omega_q \gamma_q$ gives four homogeneous equations in the coefficients t_1, t_2, t_3, t_4. The quantity Ω_q is the energy of the mixed phonon-magnon mode. The solution of the Heisenberg equation of motion is non-trivial if the following condition on the secular determinant is met:

$$\begin{vmatrix} [E(q) - \Omega_q] & 0 & \Delta_q' & \Delta_q' \\ 0 & [E(q) + \Omega_q] & \Delta_q' & \Delta_q' \\ \Delta_q'^{*} & \Delta_q'^{*} & (\hbar\omega_q - \Omega_q) & 0 \\ \Delta_q'^{*} & \Delta_q'^{*} & 0 & (\hbar\omega_q + \Omega_q) \end{vmatrix} = 0 . \quad (32)$$

In writing Equation (32) we use $\Delta_{-q}' = \Delta_q'^{*}$. The determinant may be simplified easily, and reduces to the following equation for the eigenvalues of the mixed-mode state:

$$\Omega_q^4 - \Omega_q^2 \{[E(q)]^2 + (\hbar\omega_q)^2\} + (\hbar\omega_q)^2 [E(q)]^2 - 4\hbar\omega_q |\Delta_q'|^2 E(q) = 0 . \quad (33)$$

One observes strong mixing when $E(Q) = \hbar\omega_Q$, Q being the wavenumber at which

the branches "kiss." In this case Equation (33) has the solution:

$$\Omega_Q = E(Q) \pm |\Delta_Q'| \ .$$

Then the energy splitting Δ_2 at Q is:

$$\Delta_2 = 2|\Delta_Q'| = \frac{\tilde{B}^{\epsilon}}{c} \left\{ \frac{\hbar^2 S^3 (A_Q + B_Q)}{m [E(Q)]^2} \right\}^{1/2} \sin \frac{Qc}{2} \ . \qquad (34)$$

Taking E(Q) to be 2.0 meV and Q = 0.25 Å^{-1} we find:

$$\Delta_2 = 0.86 \text{ meV.}$$

This compares well with the splitting shown in Figure 11.

SUMMARY AND CONCLUSIONS

The development of the formalism of Evenson and Liu to treat the magnetoelastic perturbation of the dynamic properties of a crystal has been a major aspect of this work. Previous ad hoc models appear in certain limits of the theory, giving a coherence to the theoretical picture of magnetoelastic coupling. In general, the local coupling theory has been successful in accounting for a large number of experiments performed on Tb and Dy metals.

The Hamiltonian of Evenson and Liu was used as a starting point, as it is a simple and physically plausible model for this interaction. It assumes that the atomic spins couple locally to the strain field. It is found that uniform magnetostriction causes a smooth transition from "free lattice" to "frozen lattice" perturbation of the magnon spectrum depending on the wavevector of the state. Manifestation of the free lattice perturbation is also limited by the finite response time of the lattice. It is found that neutron diffraction can only excite frozen lattice magnons, because the lattice is unable to respond to spin excitations spread spacially throughout the crystal. In ferromagnetic resonance studies of a metal, however, spins couple to the microwave fields within the radiation skin depth; and this skin depth is of the same magnitude as the lattice response distance for a typical spin vibration frequency. Therefore, in these microwave experiments, the free lattice response is possible.

The microwave absorption versus magnetic field applied along the hard planar axis of Tb and Dy is calculated. It is found that free lattice

magnons are primarily responsible for low frequency absorption in Tb below 140 K, and for both low and high frequency absorption in Dy below the Curie temperature of that metal. It is shown that the transition from free to frozen lattice behavior of the magnon spectrum is essential to the explanation of existing data on the temperature dependence of absorption peak positions in Tb.

The formalism of Evenson and Liu is also used to calculate the dynamic interaction between spin and lattice waves. The use of local strain functions was particularly suited to this problem since lattice waves create non-uniform local strains which are superposed on a background of uniform magnetostriction induced by the spin order. Mixed-mode energy splittings are calculated in regions of the Brillioun zone where phonon and magnon dispersion curves cross. The theory fails to account for the large splitting which occurs at the crossing point of the acoustical magnon and transverse optical phonon branches in Tb metal, but predicts well a smaller splitting which occurs where the acoustical magnon and transverse acoustical branches touch. An alternate mechanism which may account for the former splitting is given in the Appendix.

REFERENCES

1. W. C. Koehler, J. Appl. Phys. 36, 1078 (1965).
2. R. J. Elliott, Phys. Rev. 124, 346 (1961).
3. J. Villain, J. Phys. Chem. Solids 11, 303 (1959).
4. See review article by T. Kasuya, in Magnetism, edited by G. T. Rado and H. Suhl (Academic Press Inc., New York, 1966), Vol. IIB, Sec. III.
5. W. E. Evenson and S. H. Liu, Phys. Rev. 178, 783 (1969).
6. U. Enz, Physica 26, 698 (1960).
7. J. J. Rhyne and A. E. Clark, J. Appl. Phys. 38, 1379 (1967).
8. H. B. Callen and E. Callen, J. Phys. Chem. Solids 27, 1271 (1966).
9. E. Callen and H. Callen, Phys. Rev. 139, A455 (1965).
10. B. F. DeSavage and A. E. Clark, Fifth Rare Earth Conf. Ames, Iowa (1965).
11. A. E. Clark, B. F. DeSavage, and R. Bozorth, Phys. Rev. 138, A216 (1965).
12. B. R. Cooper, R. J. Elliott, S. J. Nettel, and H. Suhl, Phys. Rev. 127, 57 (1962).
13. B. R. Cooper, Phys. Rev. 169, 281 (1968).
14. E. A. Turov and V. G. Shavrov, Fiz. Tverd. Tela 7, 217 (1965) (translation: Soviet Phys. - Solid State 7, 166 (1965).
15. H. Marsh and A. J. Sievers, J. Appl. Phys. 40, 1563 (1969).
16. D. M. S. Bagguley and J. Liesegang, Proc. Roy. Soc. A300, 497 (1967).
17. F. C. Rossol, Ph.D. Thesis, Harvard University, Cambridge, Mass., 1966 (unpublished).
18. F. C. Rossol and R. V. Jones, J. Appl. Phys. 37, 1227 (1966).
19. T. K. Wagner and J. L. Stanford, Phys. Rev. 184, 505 (1969).
20. T. K. Wagner and J. L. Stanford, Phys. Rev. B1, 4488 (1970).

21. L. Hart and J. L. Stanford, Iowa State University, Ames, Iowa, Phys. Rev. Letters (to be published).

22. M. Nielsen, H. B. Møller, P. A. Lindgård, and A. R. Mackintosh, Phys. Rev. Letters 25, 1451 (1970).

23. W. P. Mason, Phys. Rev. 96, 302 (1954).

24. R. M. Bozorth, Phys. Rev. 96, 311 (1954).

25. R. Becker and W. Doring, Ferromagnetismus (Julius Springer-Verlag, Berlin, 1939).

26. H. Callen and E. Callen, J. Phys. Chem. Solids 16, 310 (1960).

27. B. F. DeSavage, M.S. Thesis, University of Maryland, College Park, Md., 1964 (unpublished).

28. H. B. Callen and E. Callen, Phys. Rev. 136, A1675 (1964).

29. B. R. Cooper, Phys. Rev. Letters 19, 900 (1967).

30. L. R. Sill and S. Legvold, Phys. Rev. 137, A1139 (1965).

31. J. J. Rhyne and S. Legvold, Phys. Rev. 138, A507 (1965).

32. E. S. Fisher and D. Dever, Trans. Met. Soc. AIME 239, 48 (1967).

33. D. R. Behrendt and S. Legvold, Phys. Rev. 109, 1544 (1958).

34. D. E. Hegland, S. Legvold, and F. H. Spedding, Phys. Rev. 131, 158 (1963).

35. T. K. Wagner and J. L. Stanford, Iowa State University, Ames, Iowa, Phys. Rev. (to be published).

36. H. B. Møller, M. Nielsen, and A. R. Mackintosh, J. Appl. Phys. 41, 1174 (1970).

37. H. B. Møller, M. Nielsen, and A. R. Mackintosh, A.E.K. Research Establishment, Risø, Denmark, J. Appl. Phys. (to be published).

38. M. S. S. Brooks, D. A. Goodings, and H. I. Ralph, J. Phys. C., ser. 2, 1, 132 (1968).

39. R. A. Reese and R. G. Barnes, Phys. Rev. 163, 465 (1967).

ACKNOWLEDGMENTS

I wish to express my sincere gratitude to Dr. S. H. Liu for his constant guidance throughout my graduate years. His fertile ideas and apt suggestions were instrumental in the production of this work. Also, I wish to thank Dr. T. K. Wagner and Mr. L. Hart for many fruitful discussions concerning ferromagnetic resonance. Finally, I am very grateful to the physics staff as a whole for providing an excellent environment for research.

APPENDIX: A MECHANISM FOR THE COUPLING OF MA AND TO MODES IN Tb

In this Appendix a mechanism is proposed which couples acoustical magnons to optical phonons along the $\hat{c}$-axis of a hcp crystal near the edge of the Brillioun zone. Such coupling results in a splitting of the dispersion relations of these modes as observed in Tb metal, and cannot be explained using a formulation of magnetoelasticity which couples the spin system to local strain fields.

In order to see how the lattice couples to the spin system, one must look in detail at the way the ions vibrate when a TO mode is excited along the c-axis near the Brillioun zone edge. One sublattice of atoms, say $f = (\ell, 0)$, remains nearly stationary; whereas, the other sublattice, $f = (\ell, c/2)$, vibrates with nearest neighbor planes on the sublattice being nearly 180^{o} out of phase. Thus, a kind of angular motion about the stationary sites is generated by the nearest neighbor ions. This net angular motion produces a magnetic field which interacts with the spins on the stationary sites. The field will be proportional to the instantaneous current created by the nearest neighbor ions moving in opposition, and will be directed perpendicular to the plane of this motion. Note that no such net field is created in a TA mode since the nearest neighbor planes are then moving in phase and no net angular moment is produced about any spin site.

The interaction created in the optical mode of vibration may be formulated as follows:

$$H_{me} = \sum_{f,\delta} \vec{H}_{f\delta} \cdot \vec{S}_f \quad . \tag{A1}$$

Here, and in all following equations, the sum on f is restricted to the sublattice $(\ell, 0)$. The quantity $\vec{H}_{f\delta}$ is the effective magnetic field generated at site f by the motion of nearest neighbors labelled by δ, and $\vec{S}_f$ is the spin on the $f^{\underline{th}}$ site. It is easily seen that the field $\vec{H}_{f\delta}$, being proportional to the current of the moving ions, is proportional to the vector angular velocity of the nearest neighbors about the $f^{\underline{th}}$ site. Therefore, Equation (A1) may be written:

$$H_{me} = \sum_{f\delta} A[(\vec{R}_f - \vec{R}_{f+\delta}) \times (\vec{v}_f - \vec{v}_{f+\delta})] \cdot \vec{S}_f \quad . \tag{A2}$$

Here $\vec{R}_f$ is the position vector of the $f^{\underline{th}}$ site, $\vec{v}_f$ is the velocity of the $f^{\underline{th}}$ site, and

$$A = \frac{24e^- \mu_B}{\pi c_0 c^3} \quad .$$

We have assumed the charge on ion = $3e^-$, and c_0 is the velocity of light. We apply Equation (A2) to Tb metal, assuming that the net magnetization is confined to the basal plane along the easy $\hat{a}$-axis. We take the polarization of the TO phonons to be in an arbitrary planar direction, specified by angle θ to the $\hat{a}$-axis. Then, assuming $\vec{v}_f \approx 0$, the part of Equation (A2) which leads to magnon-phonon mixing is given by:

$$H_{m-p} = \sum_{f\delta} (\mp) \frac{Ac}{2} v_{f+\delta} S_f^y \cos\theta \, . \tag{A3}$$

Here $(\mp)$ is used when summing on atoms in the $(^{\text{upper}}_{\text{lower}})$ nearest neighbor

planes of the $f^{\underline{th}}$ atom. The quantity c is a lattice constant. The quantity S_f^y is the component of the spin perpendicular to the â-axis, and may be expressed as a linear combination of Fourier transformed spin deviation operators of the sublattice $f = (\ell, 0)$:

$$S_f^y = i\sqrt{\frac{NS}{2}} \sum_k \left(a_k^\dagger e^{-i\vec{k}\cdot\vec{f}} - a_k e^{i\vec{k}\cdot\vec{f}}\right) .$$

Then noting that the Fourier components of the displacement $\vec{r}_{f+\delta}$ depend on time according to the factor $e^{i\omega_q t}$, we use Equation (20) to transform $\vec{v}_{f+\delta} = \frac{d}{dt}(\vec{r}_{f+\delta})$ to phonon operators. Then after summation over f and δ, Equation (A3) becomes:

$$H_{m-p} = \frac{3cAi}{2}\sqrt{NS}\cos\theta \sum_q \omega_q R_q \sin\frac{qc}{2}(\beta_{-q}^\dagger + \beta_q)(a_{-q} - a_q^\dagger) . \qquad (A4)$$

Here the optical phonon index, $\rho = 2$, is suppressed. The spin operators of Equation (A4) may be transformed to a linear combination of acoustical and optical magnon operators by using Equations (27) and (29). Then the part of Equation (A4) which couples TO phonons to MA magnons becomes:

$$H_{TO-MA} = \sum_q \Delta_q (\beta_{-q}^\dagger + \beta_q)(\alpha_{-q} - \alpha_q^\dagger) . \qquad (A5)$$

Here, the acoustical magnon index, $j = 1$, is suppressed. The strength of the interaction, Δ_q, in the region of strong coupling is written explicitly as:

$$\Delta_Q = \frac{3Ac\,i}{4}\left[\frac{S(A_Q + B_Q)}{m}\right]^{1/2} \sin\frac{Qc}{2}\,|\cos\theta| , \qquad (A6)$$

where Q is the wavenumber at which the acoustical and optical branches cross. The unperturbed TO phonons are degenerate with respect to polarization direction, so we consider θ as uniformly distributed between zero and $\pi/2$ with probability density $P(\theta) = (\frac{\pi}{2})^{-1}$. Then the splittings Δ_Q are distributed with density $P(|\cos\theta|) = 2/\pi \sin\theta$. This is reflected in the energy absorption profiles of a neutron diffraction experiment which should show sharp peaks in the neutron scattering by quasi-particles in the region of maximum splitting (i.e., for $\theta = 0$). The peak should be asymmetric, dropping sharply to zero for energies greater than that given by maximum splitting, and more gradually to a small minimum at the unperturbed energy of the phonon and magnon excitations.

One may account for the natural linewidth of the quasiparticle states by allowing the delta function distribution of each value $|\cos\theta|$ to broaden into a Lorentzian distribution. Letting $x = |\cos\theta|$, the probability density for the unbroadened spectrum is $P(x) = \int dr\ \delta(x-r)\ P(r)$. In this expression we make the replacement $\delta(x-r) \rightarrow (\gamma/\pi)[(x-x')^2 + \gamma^2/4]^{-1}$, where γ is the linewidth of the spectrum. The distribution which allows for broadening then may be written as:

$$P(x) = \frac{2\gamma}{\pi} \int_0^1 dr\ (1-r^2)^{-1/2}\ (r^2 - 2xr + x^2 + \gamma^2/4)^{-1} \quad . \qquad (A7)$$

The integral in Equation (A7) has been computed numerically and shows a strong, asymmetric peak in the region of maximum splitting ($\theta = 0$) (39). If the model proposed here has any validity, this lineshape should be a characteristic of the neutron energy absorption profiles.

Although the interaction, Equation (A1), explains in some qualitative ways the acoustical and optical mode coupling, the value of the splitting computed from Equation (A6) is much too small to account for the observed splitting in Tb. This is probably due to our simplified quasi-classical formulation which couples the local spins to an effective field produced by the lattice vibrations. A much stronger interaction might be produced if the conduction electrons mediate the interaction between the lattice and the local spins, in analogy to the strong indirect exchange interaction which couples the local spins together in Tb. Mediation by itinerant 5d electrons is plausible, since their large orbital moments can couple effectively with the field produced by the vibrating lattice.